

**Special Collection:**

Climate and weather extremes in a warming climate: Processes, Prediction and Projection

Key Points:

- No robust change in TC frequency across the region, but very strong TCs (category 4) projected to increase in frequency
- Uncertainty in TC projections mainly due to diverging patterns of SST and tropical convection in host models
- Extreme precipitation totals associated with TCs increase by 30%–35% across the region by the end-of-century under SSP370

Supporting Information:

Supporting Information may be found in the online version of this article.

Correspondence to:

P. B. Gibson,
peter.gibson@niwa.co.nz

Citation:

Gibson, P. B., Lewis, H., Campbell, I., Rampal, N., Fauchereau, N., & Harrington, L. J. (2025). Downscaled climate projections of tropical and ex-tropical cyclones over the southwest Pacific. *Journal of Geophysical Research: Atmospheres*, 130, e2025JD043833. <https://doi.org/10.1029/2025JD043833>

Received 9 MAR 2025

Accepted 4 JUL 2025

Downscaled Climate Projections of Tropical and Ex-Tropical Cyclones Over the Southwest Pacific

Peter B. Gibson¹ , Hamish Lewis^{1,2} , Isaac Campbell^{1,3} , Neelesh Rampal¹, Nicolas Fauchereau¹, and Luke J. Harrington²

¹National Institute of Water and Atmospheric Research (NIWA), Wellington, New Zealand, ²Te Aka Mātuatua School of Science, University of Waikato, Hamilton, New Zealand, ³Intelligent Earth (UKR CDT in AI for the Environment) Programme, Doctoral Training Centre, University of Oxford, Oxford, UK

Abstract Reliable projections of tropical cyclones (TCs) and associated impacts remain hampered by both climate model resolution and simulation length. To address this, here we present updated projections of TCs for the southwest Pacific from a high-resolution downscaled ensemble of CMIP6 models. The downscaling implements a variable-resolution atmospheric model enhancing resolution over the southwest Pacific and New Zealand (~12–30 km). We assess future changes in TC frequency, changes in large-scale environmental conditions, and associated extreme precipitation and winds across tropical and ex-tropical storm phases. Changes in TC track pathways are also investigated through cluster analysis. Across the downscaled simulations, robust changes in TC frequency were not found, including for a high-emissions scenario at end-of-century. Projections of the background environmental conditions are shown to be a significant source of uncertainty, owing to diverging projections of relative SST and tropical convection across the region in the host GCMs. However, very strong TCs (category 4 and above) show greater consensus for an increase in frequency, with 16 of 18 simulations across models and scenarios projecting an increase. Cluster analysis of TC tracks indicates a slight decrease in tracks that often impact northern parts of Australia. Extreme precipitation associated with TCs under a high-emissions scenario is projected to increase by ~30%–35% averaged across models, both for storms in the tropics and ex-TCs impacting New Zealand. This increase exceeds Clausius-Clapeyron scaling in five of six simulations. These projected increases in associated extreme precipitation pose significant societal risks despite the remaining uncertainty in TC frequency changes.

Plain Language Summary Our study uses a high-resolution climate model to improve tropical cyclone (TC) projections for the southwest Pacific by downscaling data from the most recent generation of global climate models. Models disagree on whether TCs will increase or decrease in frequency overall across the region, though there is stronger agreement that very strong TCs will increase in frequency. Under a high emissions scenario, by the end of century, extreme rainfall from TCs is also expected to rise by 30%–35% across the region. These findings highlight the potential for more intense TCs and heavier rainfall in the future, increasing risks for vulnerable communities across the southwest Pacific and New Zealand.

1. Introduction

Tropical cyclones (TCs) in the southwest Pacific can have devastating societal and economic impacts (Diamond et al., 2011; Walsh et al., 2012). These arise from direct TC impacts to northern parts of Australia and Pacific Island nations, as well as impacts to New Zealand from ex-tropical cyclones as they travel poleward and undergo extratropical transition (Chand et al., 2019; Harrington et al., 2023; Sinclair, 2002; Stone et al., 2024). While TCs lose structure and strength during extratropical transition, they can also re-intensify for periods of time across the mid-latitudes and produce storms with extremely damaging winds and precipitation (Sinclair, 2002). For the southwest Pacific basin, total damages can be larger during the ex-tropical phase due to impacts on the more populated regions of New Zealand (Lorrey et al., 2014).

From an economic perspective, the frequency of the highest intensity TCs is of most interest, where a relatively small number of events generally account for the majority of economic damages (Knutson et al., 2020; Mendelsohn et al., 2012; Muller et al., 2025). Notable examples of the most damaging category-5 TCs in the southwest Pacific include cyclone Winston in February 2016 (minimum pressure 884-hPa) and cyclone Pam in March 2015 (minimum pressure 896-hPa), both imposing especially large damages across the islands of Vanuatu and Fiji. For New Zealand, ex-tropical cyclones Giselle (April 1968), Bola (March 1988), and

© 2025 The Author(s).

This is an open access article under the terms of the Creative Commons Attribution-NonCommercial License, which permits use, distribution and reproduction in any medium, provided the original work is properly cited and is not used for commercial purposes.

Gabrielle (February 2023) are the most prominent historical examples of extremely damaging storms. The impacts from Cyclone Gabrielle far exceeded all previous damages from an individual storm, resulting in total estimated economic costs for New Zealand of \$14.5B NZD and general insurance claims exceeding \$1B NZD (Wilson et al., 2023).

Climatologically, the southwest Pacific basin produces approximately 9 TCs per year, with November through April marking the most active months (Diamond et al., 2011). While the southwest Pacific has fewer TCs compared to other basins (Sobel et al., 2021) it produces some of the strongest TCs globally in terms of minimum MSLP. On average, about three TCs transition south of 35°S each year, with March showing the largest proportion of ex-TC transitions (Sinclair, 2002). The South Pacific Convergence Zone (SPCZ), which extends from the equator toward the southeast across the South Pacific, provides highly favorable conditions for TC genesis in the peak summer months with abundant moisture supply and minimal vertical wind shear across the region (Brown et al., 2020). Additionally, the climatological variability in TC frequency across different timescales can be influenced by the El Niño Southern Oscillation (ENSO), the Madden-Julian Oscillation (MJO), and the Southern Annular Mode (SAM) (Diamond & Renwick, 2015a, 2015b; Diamond et al., 2013). The position of the SPCZ varies with ENSO phase to modulate favorable TC genesis locations (Brown et al., 2020), where the SPCZ position is shifted to the southwest during La Niña and to the northeast during El Niño. Historical trends in TC frequency for the entire southwest Pacific across the satellite-era (i.e., since ~1980) generally do not show robust trends (Sobel et al., 2021), though a decreasing trend has been reported for regions of Australia in certain months (Chand et al., 2019; Sobel et al., 2021).

Understanding how future TCs and ex-tropical cyclones will respond to climate change is of significant interest in both scientific and societal contexts. Results from GCM simulations suggest a slight overall global decrease in TC frequency with warming (Knutson et al., 2020). A few studies using individual high-resolution models have reported a projected increase in global TC frequency (e.g., Bhatia et al., 2018) but a conclusive physical mechanism explaining these differences remains unclear (Knutson et al., 2020). While TC frequency projections remain somewhat uncertain, there is greater consensus among studies that the maximum precipitation rates associated with TCs are projected to increase globally in a warming world, deemed “high confidence” in terms of the Intergovernmental Panel on Climate Change (IPCC) confidence levels (Seneviratne et al., 2021). Most high-resolution model simulations are also consistent in their projections of a proportional increase of intense TCs (category 4–5) and their maximum intensities (Knutson et al., 2020; Seneviratne et al., 2021).

Uncertainty is larger for basin-specific projections of TCs (Knutson et al., 2020) and targeted studies for the southwest Pacific remain especially limited, including for ex-tropical cyclones. Generally, studies report larger decreases in TC frequency projections for the southwest Pacific compared to other basins, with Walsh (2015) highlighting the importance of increased subsidence around key TC genesis regions. Using a single high-resolution GCM, Cheung and Chu (2023) found poleward shifts in the latitudes of TC genesis and ex-tropical cyclones, with this weaker in the southwest Pacific compared to other basins. Murakami et al. (2024) also found a poleward shift in “major TCs,” including across the southwest Pacific, but the spatial patterns and magnitudes varied between GCMs. Similarly, Bower and Reed (2024) show differences in the sign of ex-tropical cyclone frequency projections across the southwest Pacific from three high-resolution GCMs. Investigating potential future changes in TC track regimes is also a notable gap in the literature for the southwest Pacific, which has been extensively studied for Northern Hemisphere TC basins (e.g., Daloz et al., 2015; Knutson et al., 2022; Nakamura et al., 2017). Possible future changes in the main pathways of TC tracks, as imposed by climatological changes in the dominant steering flow from large-scale circulation (e.g., Gibson, Rampal, et al., 2024), could have large regional implications for island nations including New Zealand.

Despite major advances, faithfully representing TCs in sufficiently long (i.e., multi-decadal) climate model simulations remains a significant challenge (Knutson et al., 2020; Sobel et al., 2021). Previous studies relying on CMIP5/CMIP6 GCMs (on the order of 1.0-degree atmospheric resolution) note that these models consistently simulate too few TCs (Balaguru et al., 2020; Gibson, Stuart, et al., 2024; Sobel et al., 2021; Wehner et al., 2014). The High-Resolution Model Intercomparison Project (HighResMIP, Haarsma et al., 2016) includes several models at enhanced atmospheric resolution (~0.25-degree) which often show considerable improvements in the representation of TCs (Roberts et al., 2020a; Zhang et al., 2021). Due to these improvements, models at this resolution have been termed “TC-permitting,” in contrast to truly “TC-resolving” model resolutions which would

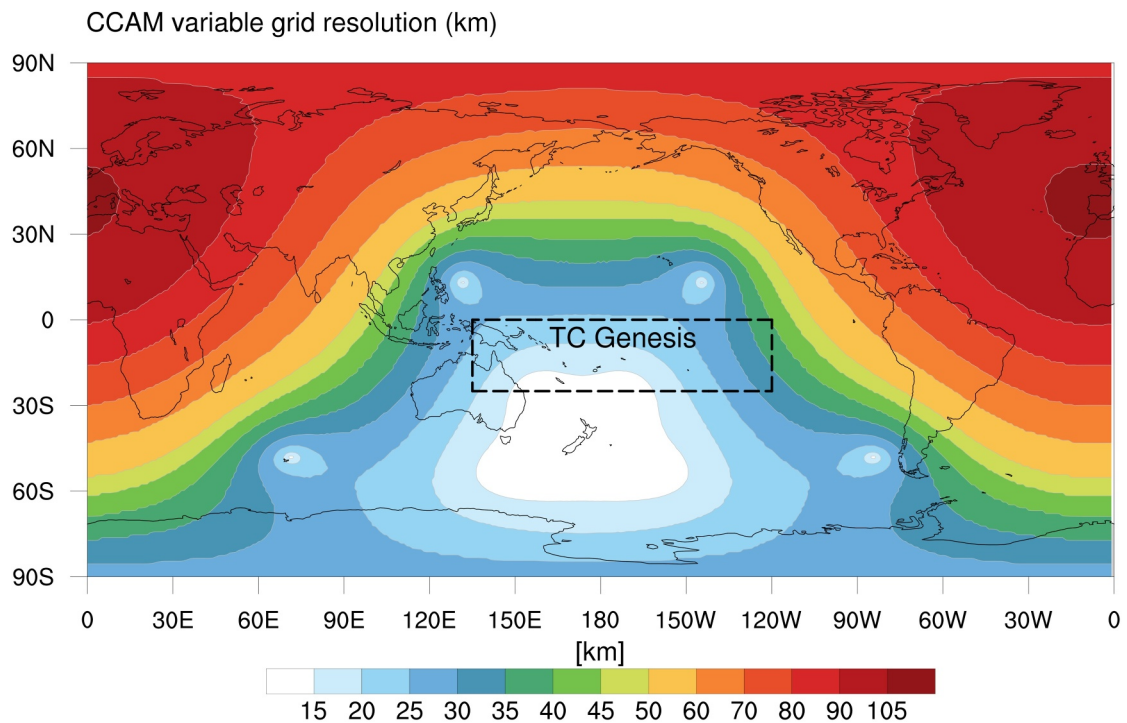


Figure 1. Grid configuration of variable-resolution downscaled CCAM simulations, where shading indicates atmospheric model resolution (units km). The TC genesis region used in this study is indicated by the boxed region with an area-average resolution of ~ 22.5 km. The highest resolution is centered over New Zealand at ~ 12 km. Figure adapted from Gibson et al. (2023).

require approximately 1 km resolution (Sobel et al., 2021). A known remaining issue with models at the TC-permitting resolution is the tendency to simulate too few very high-intensity TCs (category 4–5), although certain models can seemingly produce some events of this magnitude (Chauvin et al., 2020; Gibson, Stuart, et al., 2024; Roberts et al., 2020a; Truong et al., 2025). Since TCs are relatively rare events, particularly at the highest intensities, an ensemble with a long record of model simulations, in combination with high model resolution, is generally needed to detect a robust climate change signal (Roberts et al., 2020b).

In the present study, we present new projections of southwest Pacific TCs from a high-resolution CMIP6 downscaled ensemble. The ensemble is produced by the Conformal Cubic Atmospheric Model (CCAM), a global variable-resolution non-hydrostatic model with atmospheric resolution spanning ~ 12 – 30 km across the southwest Pacific TC basin, as documented in Gibson, Stuart, et al. (2024). Enabled by the variable-resolution grid, the model configuration targets high-resolution over New Zealand (~ 12 km) while maintaining relatively high-resolution across the broader TC basin (~ 12 – 30 km; Figure 1). Six regionally top-performing CMIP6 GCMs are downscaled by CCAM, spanning the 21st century for various shared socio-economic pathways (SSPs), providing over 1,800 model simulated years in total. To our knowledge this represents the largest ensemble at this model resolution used for TC projections in the southwest Pacific region to date. This CCAM downscaled model ensemble has been evaluated in Gibson, Stuart, et al. (2024) from the perspective of added value for various surface fields and extreme indices over New Zealand, as well as for TC frequencies over the wider southwest Pacific Basin. There it was shown that TC counts are considerably improved in CCAM relative to the host GCMs especially for higher intensity events, though these were still underrepresented in CCAM relative to observations, as characteristic of other atmospheric models at a similar resolution. The remainder of the paper is structured as follows. Details of the methodology are provided in Section 2, including the model simulations, TC tracking and TC clustering. Results and discussion are provided in Section 3 including projections of: TC frequency, large-scale environmental conditions, ex-TCs and associated changes in wind speed and precipitation.

2. Methods

2.1. Model Data

The dynamically downscaled CMIP6 model ensemble used here for climate projections of TCs is described in detail in Gibson, Stuart, et al. (2024). The ensemble is generated by CCAM, a global variable-resolution model used to downscale select CMIP6 GCMs. The grid configuration in CCAM is centered over New Zealand (~ 12 km resolution) and additionally provides relatively high-resolution ($\sim 12\text{--}30$ km) over most of the Southwest Pacific TC basin (Figure 1). Globally, the lowest resolution is in the Northern Hemisphere over parts of Europe at ~ 105 km resolution. Compared to conventional downscaling approaches with limited area regional models, this CCAM grid configuration enables a more seamless coupling between global and regional scales and may provide benefits for the representation of storms as they approach the domain of interest (Gibson et al., 2023). When driven by observed sea surface temperature (SST) and sea-ice concentration (SIC) fields, this CCAM model configuration has also been comprehensively evaluated for the southwest Pacific region in terms of climatological large-scale atmospheric circulation conditions (e.g., the jet, blocking, SAM, teleconnections, and TC statistics) (Gibson et al., 2023).

The ensemble consists of six CMIP6 GCMs downscaled with CCAM for the historical period of 1960–2014 and the “future” period of 2015–2100 across various shared socio-economic pathways (SSPs, SSP126, SSP245, SSP370). As detailed in Gibson, Stuart, et al. (2024), the GCM selection process consisted of balancing: historical period model evaluation, model independence, spread in warming rate, and data availability. Three of the six GCMs were downscaled with “spectral nudging” (Thatcher & McGregor, 2009) (ACCESS-CM2, EC-Earth3, NorESM2-MM) while three were downscaled from SST/SIC fields with input field bias correction (e.g., Chapman et al., 2023; Hoffmann et al., 2016) (AWI-CM-1-1-MR, CNRM-CM6-1, GFDL-ESM4). Within the spectral nudging approach, in terms of atmospheric fields, this was driven by 6-hourly surface pressure, winds, and air temperature at model levels between 850- and 100-hPa. Nudging was not applied to moisture fields since it is known that this can lead to physical inconsistencies between the hydrological cycle simulated by CCAM and the host model (Schroeter et al., 2024; Truong & Thatcher, 2025). For the SST/SIC driven approach, bias correction of SSTs was performed relative to OSTIA SST (1982–2014, Good et al., 2020) with the method designed to preserve temporal variability and trends from the GCM. Lastly, SIC fields were adjusted from the bias-corrected SSTs through fitting trend-preserving empirical adjustments. The reader is referred to Gibson, Stuart, et al. (2024) for additional details on both approaches.

The use of both approaches is advantageous due to data availability in CMIP6 output (i.e., SST/SIC-driven downscaling requires considerably less data than spectral nudging which is a limiting factor for many GCMs) enabling us to include more “top-performing” models and sample a wider range of warming rates in the ensemble. The use of bias corrected input SST fields was also advocated for in the context of TC projections in Sobel et al. (2021) and has been shown to improve the representation of various fields that are otherwise degraded by SST biases (Chapman et al., 2023; Hoffmann et al., 2016). Additional to the downscaled GCMs, ERA5 reanalysis (Hersbach et al., 2020) was also downscaled (years 1982–2020) with the same CCAM model configuration. This reanalysis-driven run was performed with spectral nudging to atmospheric fields from ERA5 and daily SST/SIC fields from the Operational Sea Surface Temperature and Sea Ice Analysis (OSTIA, Donlon et al., 2012).

2.2. Observational Tropical Cyclone Data

For model evaluation of TCs, two observational TC products were used as reference: IBTrACS v4 (Knapp et al., 2018) and SPEArTC (Diamond et al., 2011). SPEArTC, which is updated regularly, can be considered a reanalysis and update of IBTrACS specific to the southwest Pacific basin. It includes additional records and quality control of the tracks specific to this basin. The latitudinal range of the data set ($5^\circ\text{--}65^\circ\text{S}$) includes coverage of ex-tropical cyclones which are highly relevant to impacts for New Zealand.

2.3. Tropical Cyclone Tracking

Tempest Extremes v2.1 (Ullrich et al., 2021) was used for tracking TCs across all model simulations. An attractive feature of Tempest Extremes is that the tracking parameters are designed to work consistently across different model grid types and resolutions. To be consistent with prior studies in this region (Gibson, Stuart,

et al., 2024; Gibson et al., 2023), we have adopted similar parameters within the tracking algorithm, with further sensitivity testing detailed below.

Tracking is performed based on locating a local minimum from the 6-hrly MSLP field. A single closed contour criterion is specified, based on MSLP increasing 200-Pa over a 6-degree great circle distance from the MSLP minimum. This ensures that the low-pressure region captures a sufficiently strong, compact and coherent feature. Candidates are removed if a stronger MSLP minimum exists with a 6-degree great circle distance. When defining TC tracks, additional criteria are imposed: a track must persist for at least 60-hr, the maximum distance traveled between subsequent detections is 6-degrees, and the maximum duration between two subsequent detections is 18-hr. To focus the cyclone tracking on TCs we consider only cyclones based on genesis latitude between 0° and 25°S and we define the TC intensity/category based on MSLP along the track. The primary genesis domain used for TC tracking is 0°–25°S and 135°E–120°W, with tracking performed across the months of November through April to capture the most active TC months.

Categorization of cyclone intensity was based on the relatively simple metric of cyclone minimum central surface pressure along the track (Gibson et al., 2023; Roberts et al., 2020a), this reduces data requirements and can help improve consistency when comparing model TC tracking output against observational best track databases. It has also been shown that the cyclone minimum central pressure can serve as a better predictor of economic damages compared to maximum wind speed (Klotzbach et al., 2020; Mendelsohn et al., 2012). Following Roberts et al. (2020a), categories are defined from MSLP (hPa) ranges as: category 1 ($980 \leq x < 994$), category 2 ($965 \leq x < 980$), category 3 ($945 \leq x < 965$), category 4 ($920 \leq x < 945$), category 5 ($860 \leq x < 920$).

There is flexibility in the tracking algorithm to additionally include the presence of an upper-level warm core as a criteria in the tracking, based on geopotential height thickness computed between vertical levels (e.g., Z300 and Z500) (Ullrich et al., 2021). We found that the inclusion of a warm core criteria (vs. not) has the largest impact on the detection of TCs in the intensity range of category 1 TCs or weaker. Since the focus of this study is on stronger TCs (category 2 and above) the sensitivity to the warm core criteria is overall small. Furthermore, since we wanted to include ex-TCs in our tracking, which are highly relevant to New Zealand, the presence of a warm core criteria (which is diminished during ex-TC transitions) is considered less relevant. Subsequently, ex-TCs are defined based on the same criteria as TCs (i.e., both having genesis in tropical latitudes to distinguish from mid-latitudes cyclones), except for the fact that they transition into high latitudes. Further details are provided below for defining ex-TC related precipitation and wind speeds. As such, a warm core criterion was not used in the final tracking results presented here. We further performed sensitivity testing for how the other above-described tracking parameters (e.g., closed contour gradient threshold, track duration and distance thresholds) individually altered the frequency of tracked TCs in the downscaled ERA5 simulation. We found that most of these parameters had little influence overall on the climatological TC frequency for events that reached at least category 2 (not shown) with the largest influence for weaker tropical depressions (Roberts et al., 2020a).

Alongside the TC climatology, we consider environmental conditions from the downscaled simulations. Given their important role in TC genesis and maintenance, we assess climate projections for SSTs (positive influence) and vertical wind shear (negative influence) over the TC season. Consistent with other studies (Sobel et al., 2021), we define wind shear as the difference in windspeed between the 200- and 850-hPa pressure levels. Additionally, we compute climate projections for MSLP and precipitation over the region to further characterize changes in the TC environment. Projections of precipitation are used here for indirectly representing tropical convection changes (e.g., Brown et al., 2020; Teng & Branstator, 2017).

When defining the TC-associated precipitation and wind speed, we impose different criteria depending on the region and whether the TC has transitioned to an ex-TC. For TCs in the tropics (0°–25°S) we define their maximum precipitation rates and wind speeds as those within 2.5 degrees of the TCs central pressure and 24 hr of the TC MSLP minimum occurrence. For ex-TCs, we compute the maximum precipitation and wind rates from all points along the track, using the same 2.5-degree distance threshold, after traveling poleward of 25°S. Similarly, for ex-TCs that impact New Zealand, we compute these same maximum quantities across timesteps when the ex-TC is in the New Zealand domain (32°S–48°S, 165°E–181°E). To investigate projected changes in TC-related extremes, we define an intensification ratio as the climatology of these extremes in the future period (under SSP370, years 2070–2099) divided by the historical climatology (years 1985–2014). To account for sampling uncertainty, we additionally compute the interquartile range of these projected changes by taking 1,000 bootstrap samples (with replacement) of these extreme events across the historical and future period.

2.4. Track Clusters

To characterize the main types of TC genesis locations and tracks in the basin, as well as their projected changes, clustering was performed on the TC track output from the downscaled simulations. Polynomial regression mixture models were used which involve a probabilistic Bayesian approach to clustering whereby a polynomial model (quadratic) is regressed onto TC tracks (Camargo et al., 2007; Gaffney et al., 2007; Nakamura et al., 2017). Cluster membership is assigned based on the probability that a given TC track was generated by the cluster regression model. A notable advantage of this approach is that clustering is performed directly on the full “trajectory-space,” as opposed to on vectors of a fixed length as required under k-means clustering (Gaffney et al., 2007). The approach allows for both genesis location and TC track shape aspects to be considered collectively when defining clusters.

The clusters were generated from 1,200 TC tracks sampled from the downscaled simulations (across all GCMs) from the historical and SSP370 experiment. The high emissions scenario was included here to include possible changes to the genesis locations or TC tracks induced by a relatively strong climate change signal. Sensitivity testing revealed that 1,200 tracks was sufficient for defining these clusters, with very little variation in the clusters from including additional tracks (not shown). The clustering requires choosing *a priori* the number of clusters (k). This was done based on visual interpretation of the clusters combined with testing the sensitivity to various configurations. Following this, we present $k = 3$ as the primary cluster configuration, since adding additional clusters (e.g., $k = 6, k = 9$) tended to focus on sub-clusters that were considered of secondary importance given the primary objectives of our analysis (Figures S1 and S2 in Supporting Information S1). In particular, when $k = 6$ is implemented, additional subclusters are included to characterize smaller details of the TC genesis and tracks east of the dateline. Given their location, these have little impact on New Zealand, so the added complexity of these additional clusters was not considered beneficial. To ensure robustness of our results we further performed sensitivity testing to the choice of k in the context of future projections, which we discuss in Section 3.3.

To further test the general representativeness of these clusters ($k = 3$), TC tracks from ERA5 were projected onto the clusters derived from the downscaled GCM simulations (Figure S3 in Supporting Information S1). As shown, the ERA5 TC tracks project well onto the derived clusters, with a number of TC cases assigned to each cluster to indicate that each of these can represent realistic track orientations. When analysing future projections from the clusters, various aspects were considered on a per-model and per-cluster basis. These included the occurrence frequency of each cluster, the occurrence frequency of ex-TCs that impact New Zealand, and the average translation speed of TCs.

3. Results and Discussion

3.1. Tropical Cyclone Frequency

We begin by comparing the historical frequency of TCs and the spatial distribution of TC tracks across the downscaled simulations and observations (Figure 2). Focusing on storms that reach at least category 2 intensity, observational data sets (IBTrACS and SPEArTC) indicate a peak in climatological TC occurrence to the east of Australia between 150°E and 180°, near the islands of Vanuatu. Over this historical period (1985–2014) there were approximately 160 storms reaching this intensity. As shown in Figure 2, these storms can travel south to impact northern parts of New Zealand and are investigated in greater detail in later sections. Most of the downscaled simulations can capture the general spatial pattern of the peak TC pattern in the tropics and the potential for ex-tropical transitions which impact New Zealand. A notable difference is that ACCESS-CM2 has an eastward bias in peak TC frequency centered near 180°. Furthermore, the peak TC region in observations also encompasses more northern parts of Australia, whereas the peak TC region in the downscaled models is positioned more to the east of Australia. In terms of TC frequency, all downscaled models simulate more TCs than observed. The extent of this differs across models, with EC-Earth3 simulating the highest frequency ($N = 366$). The downscaled simulations with SST bias correction performed (i.e., AWI-CM-1-1-MR, CNRM-CM6-1, GFDL-ESM4) overall show a closer match in TC frequency relative to observations (see Figure 2 for details), with these improvements likely stemming from the reduction in SST biases in these models.

The spatial patterns of TC genesis are shown in Figure 3, along with the climatological SSTs from each model. As above, we restrict our analysis here to storms that reach at least category 2 intensity at some point in their lifetime. As described earlier for the TC tracks, ACCESS-CM2 and EC-Earth3 have a spatially extended peak of TC

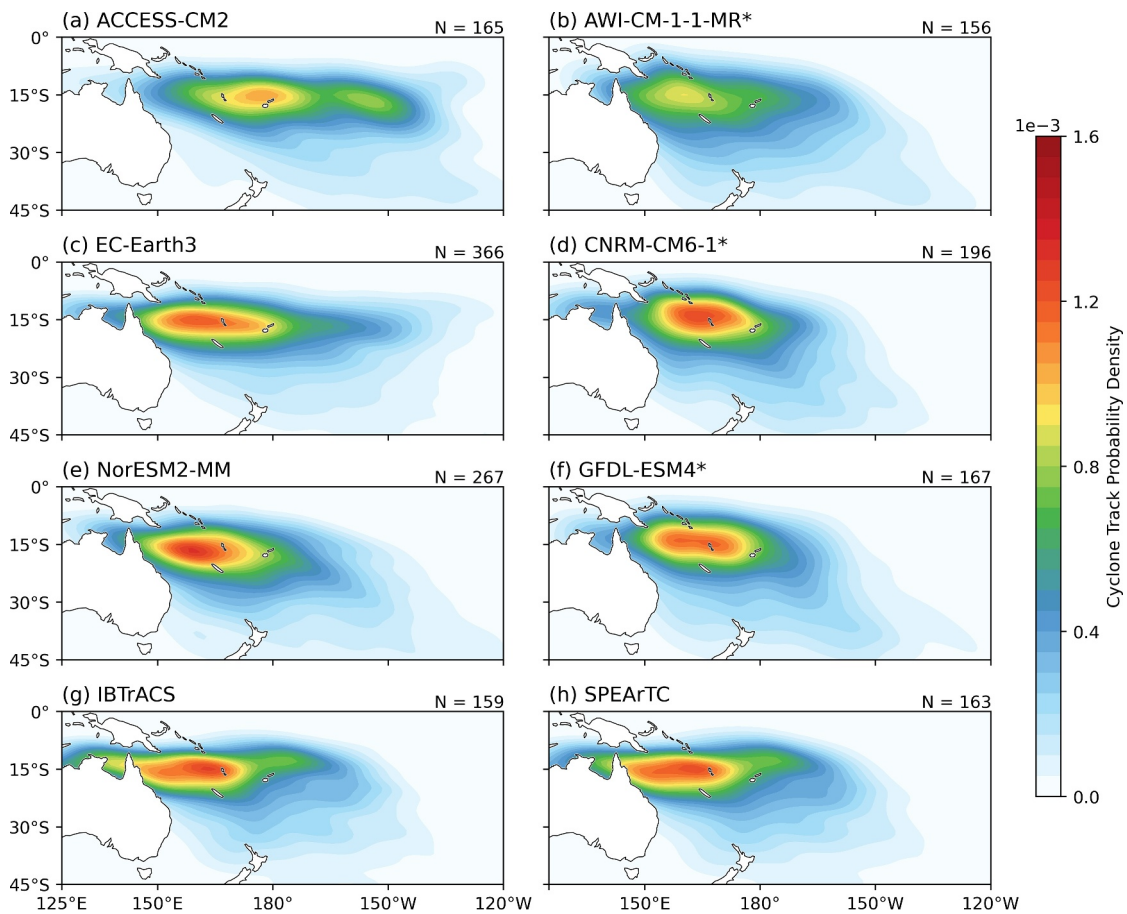


Figure 2. Heatmaps for the probability density (colors) of TC tracks over for the historical period (1985–2014, November through April) for storms that reach category 2+ intensity. The number of TCs occurring during this period is shown above each panel. IBTrACs and SPEArTC are shown in panel (g, h) as observational reference products. SST-driven models are denoted with an asterisk. Details of the other tracking criteria (e.g., a TC track must persist for at least 60-hr) are provided in Section 2.3.

genesis east of 180°E which is not found in observations. This appears driven by a warm bias in SSTs in this region, promoting excessively favorable conditions for TCs. The western Pacific warm pool is typically defined by SSTs exceeding 28°C in the present climate, where deep convection often occurs (Brown et al., 2020; Hoyos & Webster, 2012; Johnson & Xie, 2010). Biases are evident in the 28°C SST climatological isotherm in these two models which extends much further to the east compared to observations, creating a larger warm pool region. The extent of the SST bias is largest in EC-Earth3, which also likely contributes to this model having the largest frequency (i.e., positive bias) of TCs. As expected, the three SST-driven models which have had their input field SSTs bias corrected prior to downscaling have identical SST climatologies to observations (Figure 3g).

Before moving to future projections, we next extend our evaluation of historical TC frequency to higher intensity TC categories (Figure 4). We also evaluate ERA5 with and without downscaling from CCAM. The two observational products (IBTrACs and SPEArTC) are shown to produce very similar TC frequency climatologies across the different TC intensity categories for this time period. Relative to these observational products, ERA5 (without downscaling) generally simulates too few high intensity TCs, especially across categories 3+ and 4+. This under-representation for ERA5 (and other reanalysis) is consistent with previous studies in other TC basins (Gibson et al., 2023; Hodges et al., 2017; Ullrich et al., 2021). When ERA5 is downscaled with CCAM, the frequency of TCs consistently increases, this improves the under-representation of the strongest TCs overall but appears to produce too many weaker TCs, consistent with previous results using CCAM (Gibson, Stuart, et al., 2024; Gibson et al., 2023). In terms of CCAM downscaling GCMs, consistent with our earlier findings in the category 2+ intensity range (Figures 2 and 3), large differences in TC counts are evident across the GCMs, with EC-Earth3 and NorESM2-MM consistently simulating the largest number of TCs across the different TC

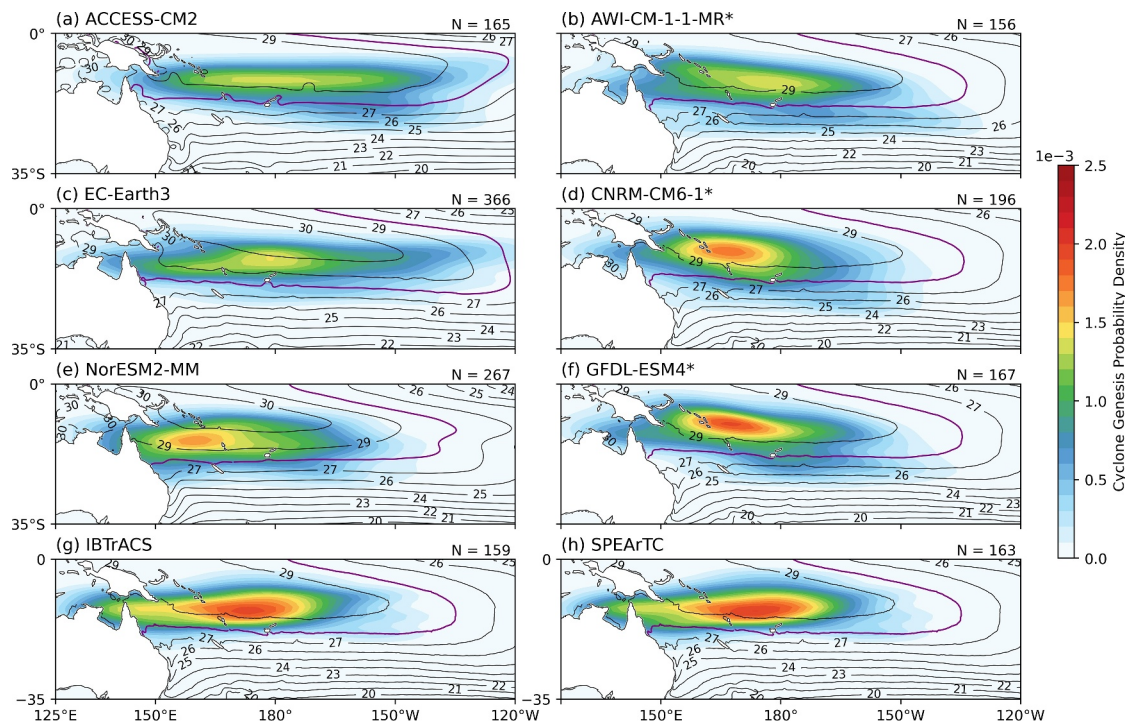


Figure 3. Heatmaps for the probability density (colors) of TC genesis over for the historical period (1985–2014, November through April) for storms that reach category 2+ intensity. Contours indicate the November through April climatological SST at intervals of 1°C and the number of TCs occurring during the historical period is shown above each panel. The 28°C contour is highlighted in purple. IBTrACs and SPEArTC are shown in panel (g, h) as the observational reference products overlaid with climatological SST contours from OSTIA. SST driven models are denoted with an asterisk.

intensities. Overall, the downscaled GCMs provide the closest match to observations in the category 2+ range (Figure 4a), whereas for higher intensity storms (Figures 4b and 4c) the models tend to underestimate frequency, consistent with findings from other TC-permitting model resolution studies (Sobel et al., 2021). Importantly, as shown in Gibson, Stuart, et al. (2024), despite these limitations, the downscaled simulations have a much better overall representation of TCs relative to TCs from the output of the lower-resolution host GCMs.

Future projections of TCs across various SSPs are shown on a per-model basis in Figure 4. For TCs in the category 2+ and category 3+ range (Figure 4b) there is a lack of model agreement concerning the sign of the projected TC frequency. For example, certain downscaled models project a slight increase in frequency (e.g., ACCESS-CM2) under the highest emissions scenario evaluated (i.e., SSP370) while others project a decrease (e.g., GFDL-ESM4). Only for very strong TCs (i.e., cat4+) is there greater consensus for an increase in frequency (Figure 4c), with 16 of 18 simulations across SSPs and models projecting an increase. For certain models (e.g., ACCESS-CM2, NorESM2-MM) this increase is substantial and roughly equates to a doubling in frequency of the very strong events under SSP370. These findings should be interpreted with the caveat that these are rare events (hence difficult to sample statistically) and that all downscaled simulations underestimate the frequency of these events to some extent. Nevertheless, the finding of a stronger consensus for a proportional increase in frequency of very strong TCs is consistent with other studies in other TC basins (Knutson et al., 2020; Seneviratne et al., 2021).

3.2. Environmental Conditions

Given the often-large differences in TC frequency projections across models (Figure 4), we next explore the potential influences from changing environmental conditions, including regional SSTs and associated gradients, tropical convection, subsidence, and wind shear. Here subsidence refers to the environmental large-scale circulation conditions, such as through changes in the Hadley cell or MSLP patterns more generally. In this section we primarily focus on changes in TC genesis in the tropics, while changes in ex-tropical cyclones and tracks are presented in Section 3.3.

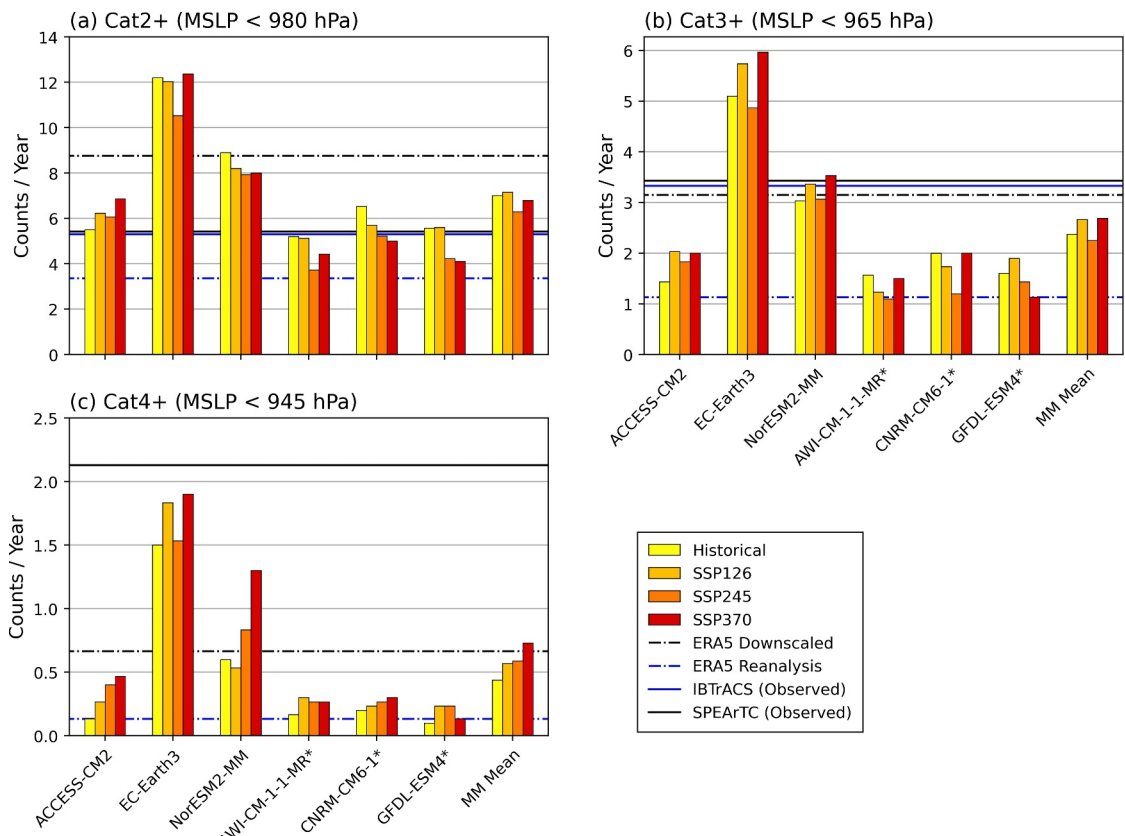


Figure 4. Frequency of TCs over the period of 1985–2014 (November through April) for the historical period, and 2070–2099 for each SSP. Panels (a)–(c) indicate different TC intensity thresholds based on MSLP minima. Bars indicate the frequencies for each downscaled model used in this study, as well as the multi-model mean. Dashed black lines indicating the frequency for the ERA5 CCAM downscaled simulation and dashed blue lines indicating the frequency of the raw ERA5 reanalysis. Solid lines indicate the frequency the observed products SPEArTC (black) and IBTrACS (blue). SST driven models are denoted with an asterisk.

Projections of TC genesis probability are shown alongside SST changes on per-model basis in Figure 5. Across models, there is little consistency in the spatial patterns of the TC genesis change maps. Resultingly, projections of TC frequency for individual Pacific Island nations are generally not considered to be robust, both from the perspective of TC genesis changes (Figure 5) and in terms of TC track frequency changes (not shown). The absolute magnitude of regional SST warming across models is shown not to be a strong predictor of increasing TC genesis probability. For example, ACCESS-CM2 has the strongest SST warming and the largest overall increase in TC frequency, yet CNRM-CM6-1 has the second strongest SST warming and the largest decrease in TC frequency. Warming SSTs alone are not expected to equate to greater TC genesis since the threshold for TC genesis also rises with warming as the troposphere warms moist adiabatically (Johnson & Xie, 2010). Instead, with warming, TCs will tend to preferably form in the warmest ocean regions in a given climate (Sobel et al., 2021).

Changes in relative SST patterns are shown in Figure 6, based on removing the regionally averaged SST warming to highlight changes in the spatial patterns of SST projections. The relative SST change maps show some consistent features across models. Namely all models tend to project relatively large increases in SSTs across the Niño3.4 region, and to a lesser extent over the Niño4 region in the central Pacific (EC-Earth3 being the notable exception). While details of the SST change pattern vary across models, these broadly resemble an El Niño like state in most models and are accompanied by cooling directly to the south (between 10°–30°S and 150°W–120°W). A notable difference is that warming is also enhanced in most models in the region to the east of Australia and just north of New Zealand, which is more characteristic of La Niña. Generally, El Niño is expected to increase TC genesis in the central Pacific and decrease TC genesis over the coral Sea and northern parts of Australia, with the reverse pattern expected under La Niña (Diamond et al., 2013). However, this El Niño-like TC response is only evident in a few of the models, most notably AWI-CM-1-1-MR. In contrast, ACCESS-CM2

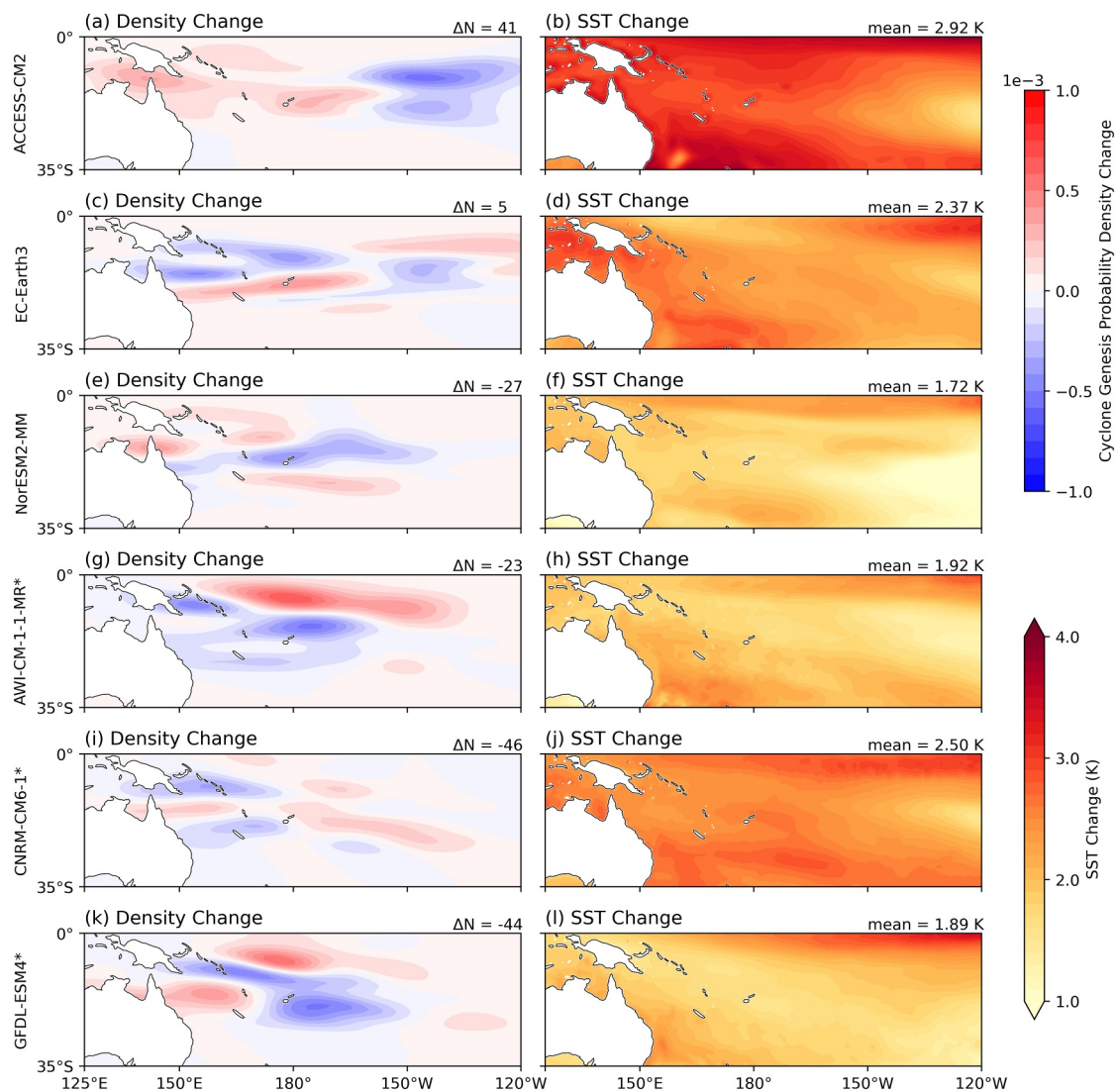


Figure 5. Changes in TC genesis probability density (category 2+) alongside the change in SST climatology for each model (SSP370 years 2070–2099 minus historical years 1985–2014, November through April). The change in TC frequency (ΔN) between future and historical periods within the domain is shown on the left panels, changes in the domain-mean SST is given on the right panels. SST driven models are denoted with an asterisk.

bears closer resemblance to a La Niña-like TC response. Clearly changes in projected SST patterns are overall limited in terms of explaining changing TC genesis regions. The strongest positive relationships between SST changes and TC genesis changes are found in ACCESS-CM2 and GFDL-ESM2, with pattern correlations in the 0.2–0.4 range, while other models have pattern correlations less than 0.1.

Changes in precipitation patterns are shown in Figure 7, used here for indirectly representing tropical convection. Overall, the changes in precipitation patterns are shown to be a much better predictor of changes in TC genesis regions, with positive pattern correlations across the models typically in the 0.3–0.5 range (except for NorESM2-MM). Given the importance of the SPCZ for providing favorable conditions for TC genesis, model projected changes across this region are highly relevant. Generally, regions with enhanced tropical precipitation (associated with enhanced tropical convection) in the future coincide with enhanced TC genesis. Similarly, regions of reduced tropical precipitation generally coincide with regions of reduced TC genesis. However, as shown earlier for the SST changes, the downscaled models project a wide range of possible precipitation change patterns with relatively little consistency, contributing to the projection uncertainty in TC genesis regions.

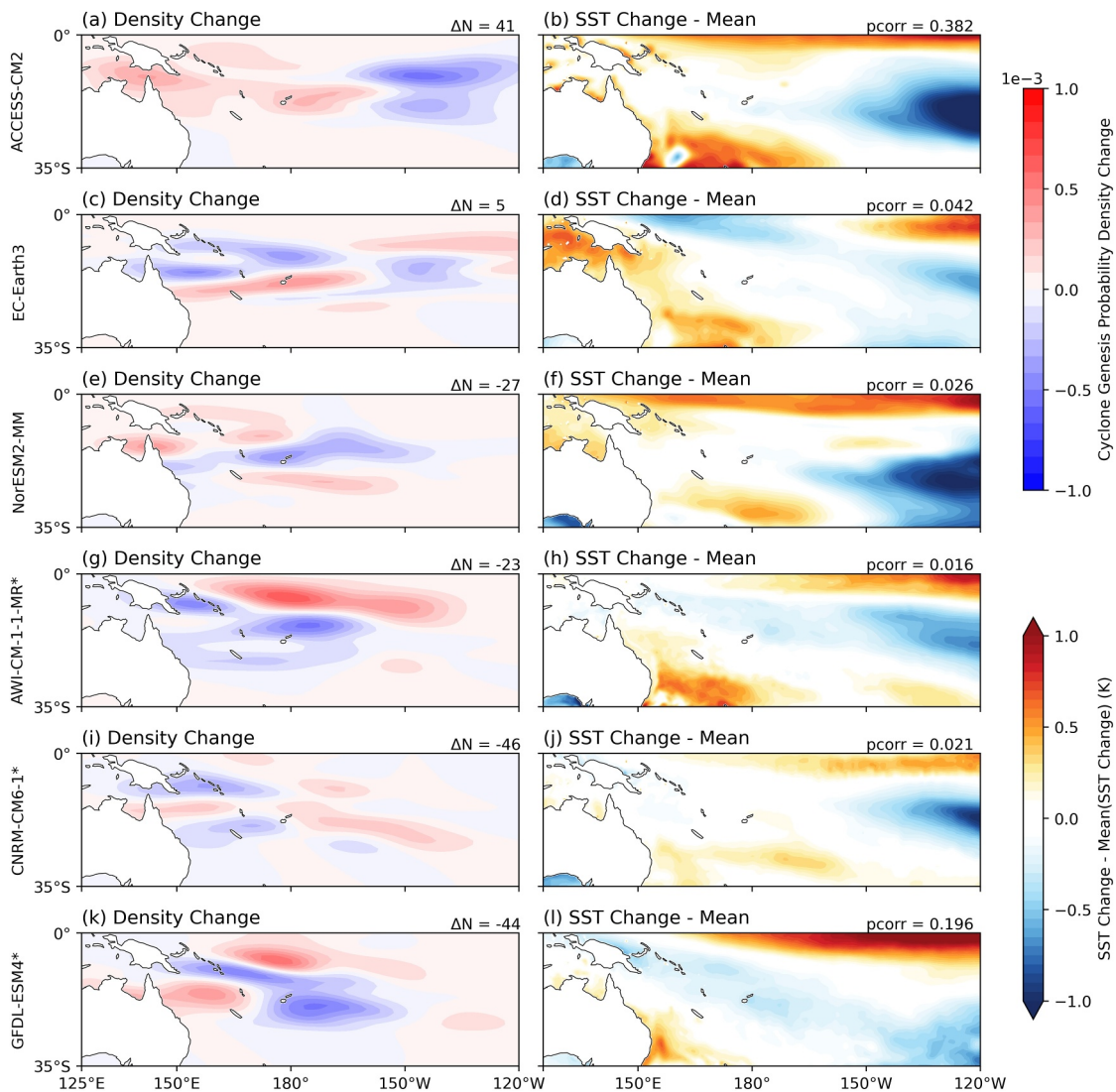


Figure 6. As in Figure 5 but here the right panels (b, d, f, h, j, l) show the change in SST after the regionally averaged SST (over the domain shown) has been removed to illustrate changes in the spatial pattern. Additionally, the pattern correlation (pcorr) between the TC density change field and the SST change field is shown on a per model basis. SST driven models are denoted with an asterisk.

Changes in wind shear and MSLP patterns are shown in Figure 8 and Figure S4 in Supporting Information S1, respectively. Higher wind shear is generally an inhibitive factor for TC genesis, therefore future increases in wind shear in key regions could act to suppress TC genesis. Compared to SST and precipitation changes shown earlier, wind shear changes generally show greater consistency across models in the southwest Pacific domain. Notably, there is a consistent pattern of decreasing wind shear in the central tropical Pacific and increasing wind shear to the south of this (approximately 10°–30°S). Although model consensus reduces over the key TC genesis region, four of the six models show projections of enhanced wind shear in this region (the exceptions being EC-Earth3 and CNRM-CM6-1 which both show relatively little change). As expected, there is generally a negative correlation between changes in wind shear and changes in TC genesis across models, except for CNRM-CM6-1 which shows a weak positive correlation. The weak positive correlation in this model, combined with a spatially noisy change signal in TCs (i.e., with no clear spatial pattern), suggests that large-scale changes in wind shear are not playing a dominant role in this particular model. In terms of MSLP changes (Figure S4 in Supporting Information S1), while models show differences in the projected spatial pattern, all models show a projected increase in MSLP in the key TC genesis region which through surface level atmospheric subsidence could act to inhibit TC genesis.

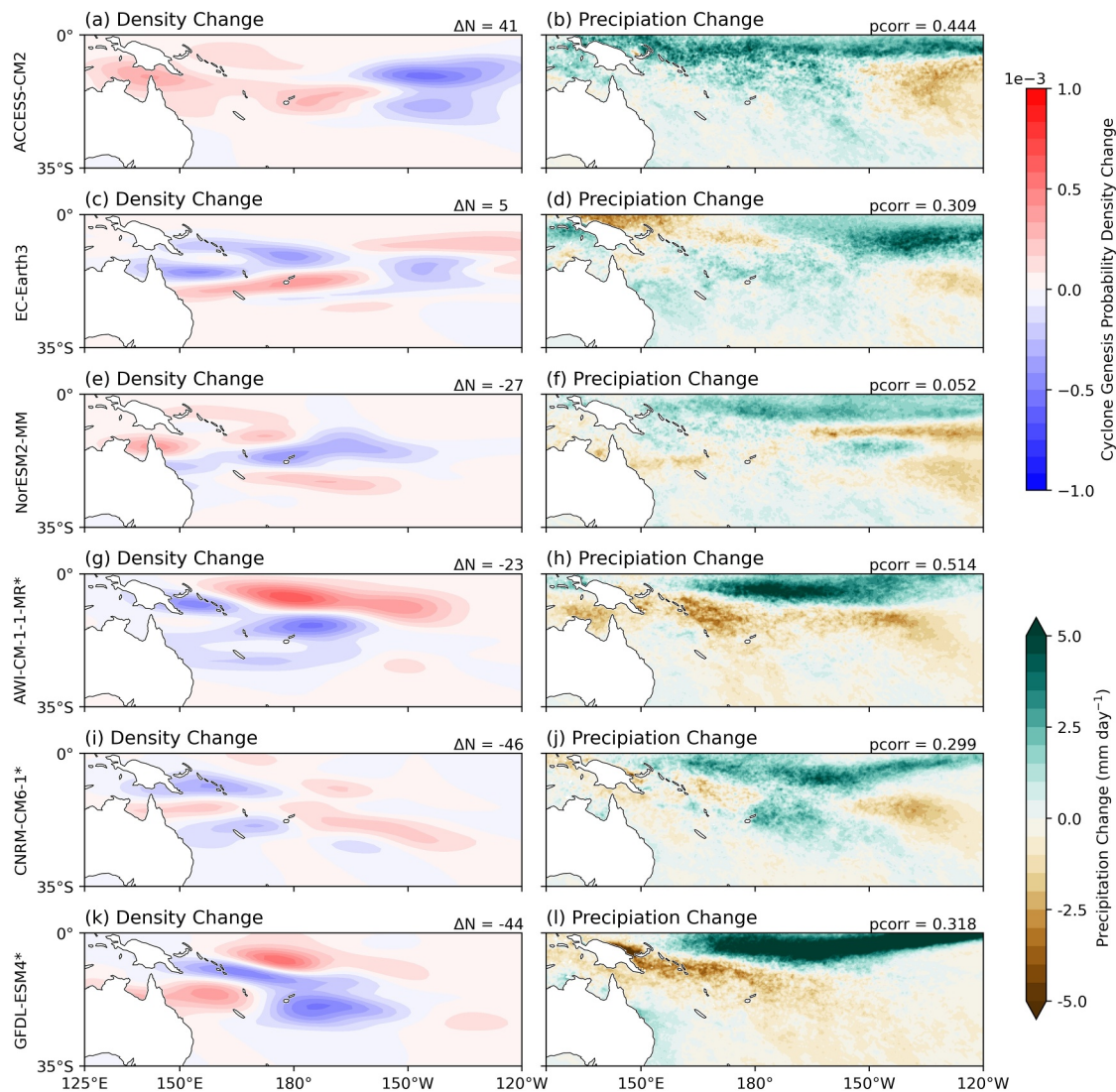


Figure 7. As in Figure 5 but here the right panels (b, d, f, h, j, l) show the change in precipitation. The pattern correlation (pcorr) between the TC density change field and the precipitation change field is shown on a per model basis. SST driven models are denoted with an asterisk.

To summarize the projected changes in environmental conditions, there is evidence that projected changes in subsidence (increasing) and wind shear (increasing) could overall act to reduce TC formation in the key genesis region. However, sign changes in convection and SST warming patterns are more mixed across models contributing to greater uncertainty in the spatial pattern and overall sign of projected TC genesis in the region. The important implications of SST pattern uncertainty on TC projection uncertainty have been emphasized in previous studies using pseudo global warming downscaling simulations from earlier CMIP5 models (Dutheil et al., 2020). Similarly, Brown et al. (2020) highlight the uncertainty in projections of the SPCZ that has persisted across generations of CMIP, with climate models disagreeing on the sign changes of precipitation in this region (i.e., whether precipitation will increase or decrease). Our finding that enhanced subsidence in the key TC genesis regions plays a contributing role (i.e., decreasing TC genesis) is also consistent with the earlier study of Walsh (2015) who used the CMIP3-derived SST change pattern to force a high-resolution regional model. Our findings add to this earlier result by showing the importance of other environmental factors and the relative uncertainties across a number of the current generation CMIP6 models. Notably, how patterns of relative SSTs and tropical convection change and their uncertainty across the host CMIP6 models in this region appears to be a leading cause for the remaining uncertainty in the downscaled TC projections.

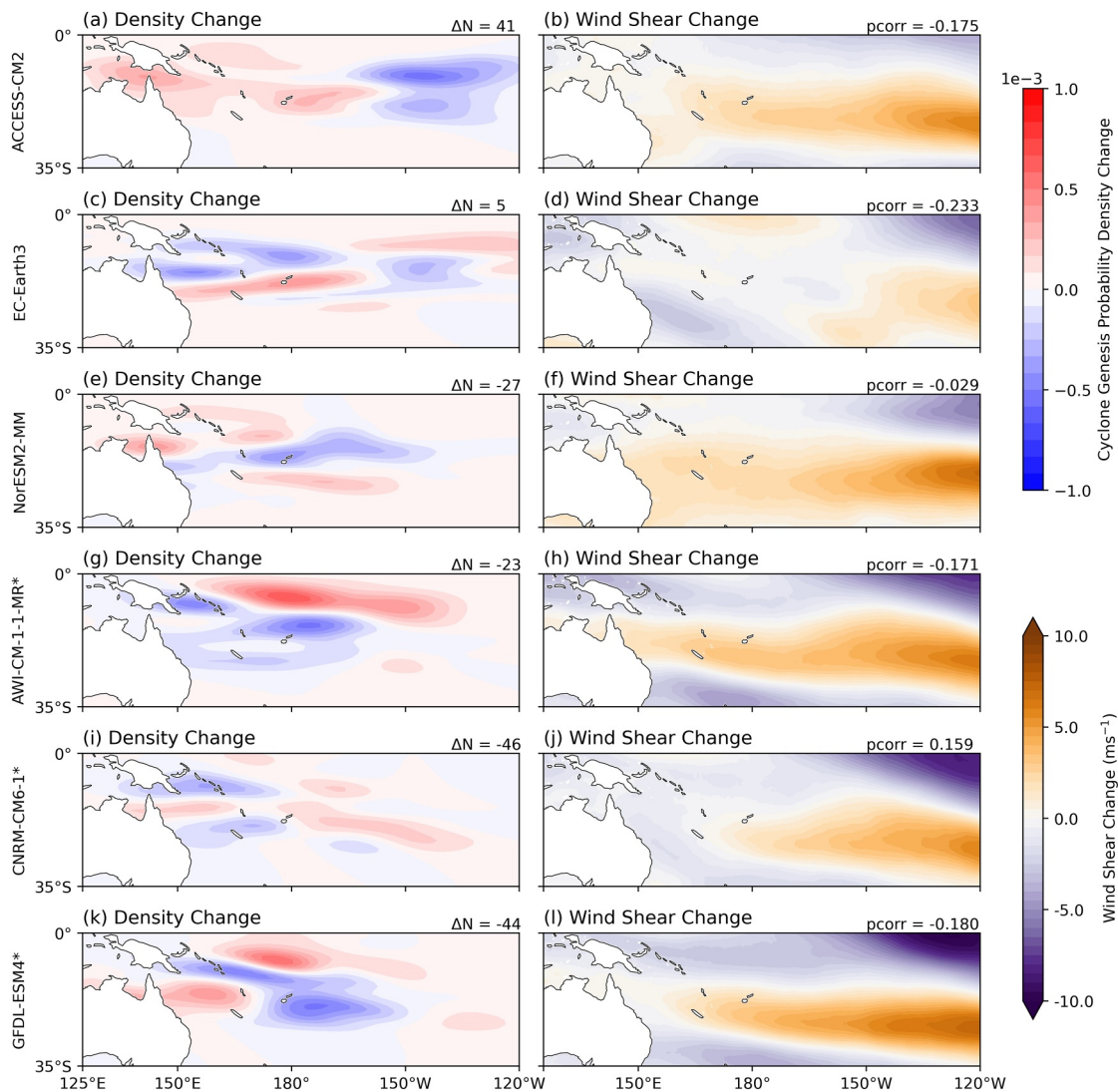


Figure 8. As in Figure 5 but here the right panels (b, d, f, h, j, l) show the change in vertical wind shear. The pattern correlation (pcorr) between the TC density change field and the wind shear change field is shown on a per model basis. SST driven models are denoted with an asterisk.

It is further possible that the projection uncertainty as presented and discussed here (e.g., Figures 4–8) is under sampling the plausible future uncertainty. Most CMIP6 models project a trend toward a more El Nino state over the next several decades despite observations over the last 50 years showing the opposite, with this difference seemingly not explainable by internal variability alone (Sobel et al., 2023; Zhuo et al., 2025). As such, the fact that future projections from CMIP6 strongly favor a future El Nino state compared to La Nina (Erickson & Patricola, 2023), may mean that projections of TC derived from downscaled CMIP6 models will incur biases from not adequately sampling future La Nina states. This could have direct and important implications for TC projections over Pacific Islands in the southwest Pacific but is arguably less important for projections of ex-tropical cyclones and their impacts on New Zealand, given the historically weaker and less direct relationship with ENSO phase in this region (Diamond et al., 2013; Lorrey et al., 2014).

3.3. Ex-Tropical Cyclones and Tracks

As discussed in Section 1, ex-tropical cyclones can impose major damages to New Zealand. In this section we study projected changes in the frequency of these events as well as changes to their typical tracks. As shown in Figure 9, observational products show that around 1 ex-TC typically impacts New Zealand per year (long-term average of 1.3/year), in general agreement with previous studies (Lorrey et al., 2014). Over the historical period,

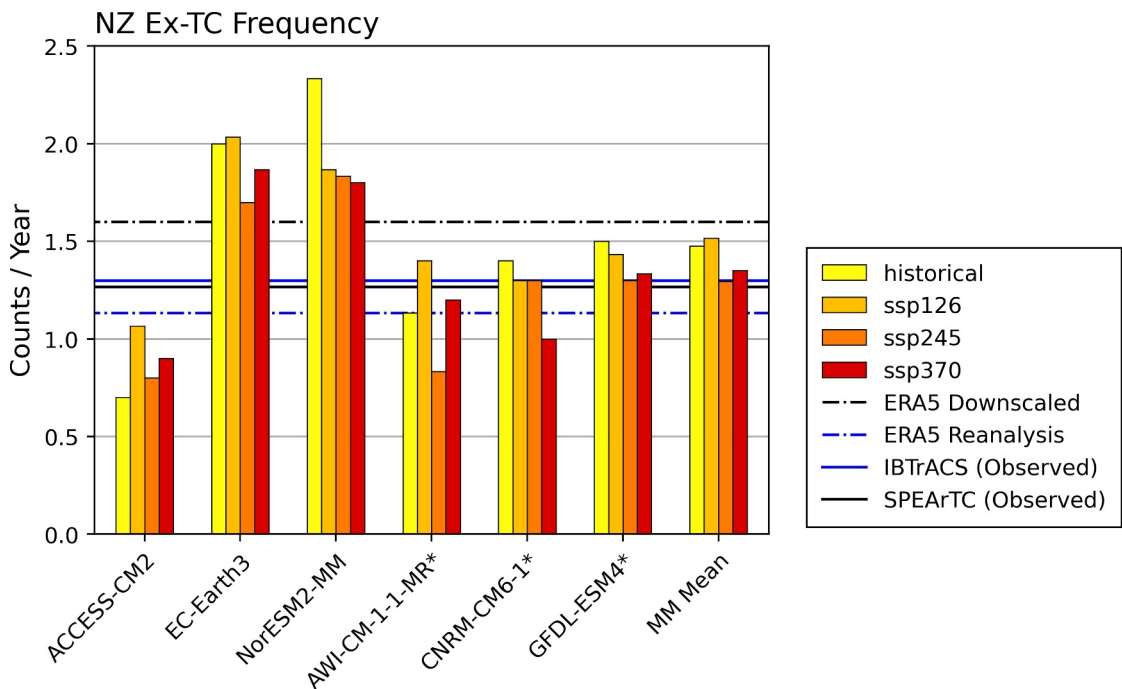


Figure 9. As in Figure 4 but here showing the frequency of ex-tropical cyclones (which reach category 2+ intensity at least once along track) which impact New Zealand (region: 48°S–32°S and 165°E–181°E, November through April). SST driven models are denoted with an asterisk.

the ensemble mean of the downscaled simulations is a reasonably good match to this, despite some models overestimating (e.g., NorESM2-MM simulates over 2 ex-TCs per year impacting New Zealand) or underestimating (e.g., ACCESS-CM2) this frequency. Notably, the SST-driven CCAM simulations appear to be more

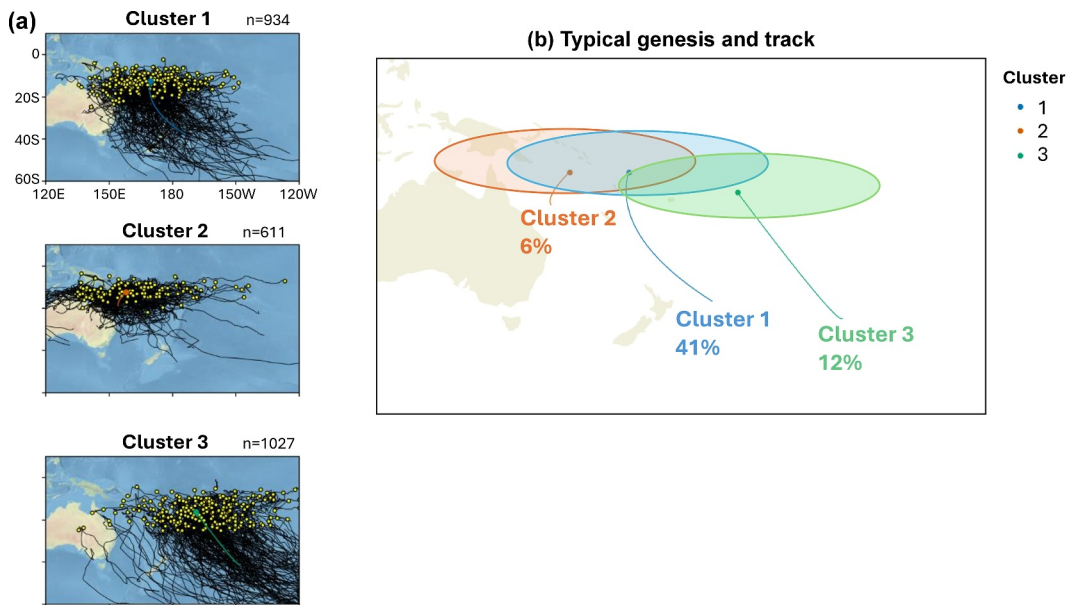


Figure 10. Clustering of TC tracks for storms that reach at least category 2+ intensity. Panel (a) shows the genesis locations in each cluster (yellow points), the individual track paths (black lines), and the cluster mean track paths (colored lines). Panel (b) is a schematic summarizing the typical genesis locations of TCs in each cluster (shaded ellipse) and the mean track paths (colored lines). Percentages in panel (b) refer to the percentage of tracks in each cluster that impact New Zealand, indicating the highest relevance of Cluster 1.

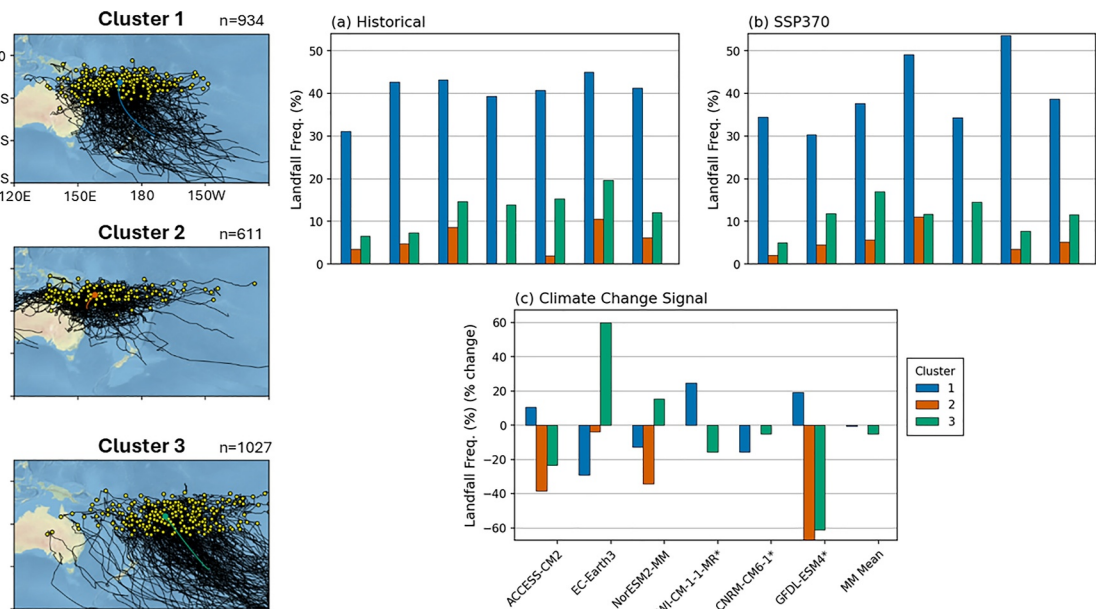


Figure 11. The frequency of TCs in each cluster that impact the New Zealand region over the historical period (panel a, years 1985–2014), the end-of-century under SSP370 (panel b, years 2070–2099) and relative percentage change future minus historical (panel c). The clusters are shown on the left-hand side for reference from Figure 10.

consistent overall with observations, in part likely due to input SST bias correction performed for these simulations.

In terms of future projections of ex-TC frequency impacting New Zealand, there is little consensus across models, with many models showing very little change across SSPs. Although four of the six models show slight decreases in frequency under SSP370, given that the climatological frequency of these events is low, we interpret the projections as showing no strong robust frequency changes in either direction. This finding is somewhat expected, given the uncertainty in TC projections shown earlier for events of this magnitude across the wider southwest Pacific basin (Figure 4a).

Since it is possible that certain aspects of projected changes could be masked by these regionally aggregated TC counts, we next delve deeper into the projected changes in TC tracks themselves. As described in Section 2, cluster analysis was performed on the TC tracks to group common genesis locations and track pathways, with the three primary clusters shown in Figure 10. Cluster 1 TCs have the largest likelihood of transitioning to ex-TCs and impacting the New Zealand region (>40%). In contrast, few of the Cluster 2 TCs transition out of the tropics, while they can still have direct impacts to northern Australia, very few impact the New Zealand region (~6%). Lastly, Cluster 3 TCs tend to have genesis further to the east and track toward the southeast, such that most of these events are too far to the east of New Zealand to have impacts when they transition to ex-TCs (~12% impact New Zealand).

The high relevance of Cluster 1 TCs to New Zealand is further illustrated under the historical period in Figure 11a. The relevance of this cluster is relatively stable under future climate change (comparing Figures 11a and 11b), implying an absence of robust shifts within the regimes into the future. Another possibility is that the frequency of these TC clusters changes into the future (Figure 12). This could potentially arise due to projected changes in regions of tropical convection which favor certain TC genesis regions (Diamond & Renwick, 2015a, 2015b) or through possible changes in the summer large scale circulation features to impact the steering of TC tracks (Gibson, Stuart, et al., 2024). The most consistent projection across models (five of six simulations under SSP370) is for a decrease in Cluster 2 TCs, implying a decrease in TCs with genesis over the more western part of the TC basin. This was also found for other cluster configurations (e.g., $k = 6$), where TCs with genesis over northern Australia and the Coral Sea, and those which typically have little impact to New Zealand due to a tendency to travel eastward over northern Australia, show the largest and most consistent projected decrease in TC frequency (Figure S5 in Supporting Information S1). Given the relevance of cluster 2 TCs to northern parts of

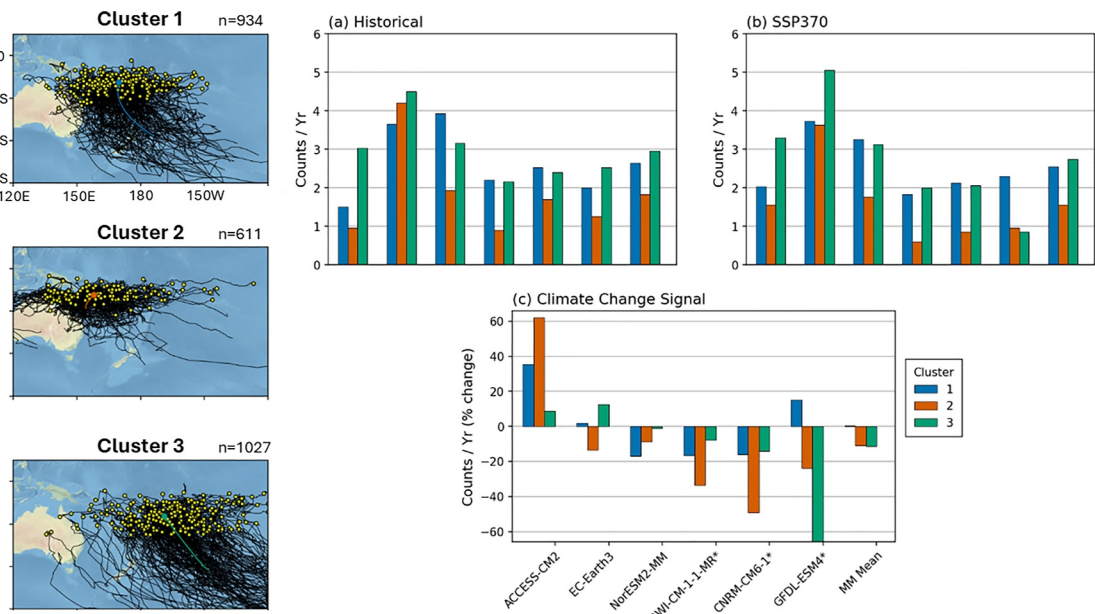


Figure 12. As in Figure 11 but here showing projections of the TC frequency on a per cluster basis irrespective of whether the storm impacts New Zealand (panels a–c). The clusters are shown on the left-hand side for reference from Figure 10.

Australia, a decrease in these events could have important implications for that region. This projected decrease is likely driven by the projected increase in wind shear and subsidence found in most downscaled models in that region, as discussed earlier in Section 3.2 and broadly consistent with the projections detailed in Walsh (2015).

Studies in Northern Hemisphere TC basins have reported important projected shifts in track latitudes with warming (e.g., Murakami et al., 2024; Nakamura et al., 2017). For the Southern Hemisphere, a poleward shift in atmospheric rivers and storm tracks have also been shown in individual GCMs (Ma et al., 2020). Similarly, using a single high-resolution GCM, Cheung and Chu (2023) found poleward shifts in the latitudes of TC genesis and ex-tropical cyclones, though this was not statistically significant over the south Pacific. In analysing poleward shifts in TC genesis regions (Figure S6 in Supporting Information S1) and TC tracks overall (Figure S7 in Supporting Information S1) we also do not find robust evidence for a shift, with changes shown to be strongly model dependent. Namely, only two models (ACCESS-CM2 and CNRM-CM6-1) show some evidence of a projected poleward shift in TC genesis, and only CNRM-CM6-1 shows clear evidence of a poleward shift in TC tracks which is mostly confined to the tropics and subtropics (i.e., equatorward of 30°S).

We also investigated changes in TC translation speed on a per cluster basis, however the projected changes were relatively small (between 1% and 4% in the ensemble mean) and inconsistent in sign across models (not shown). This lack of a robust signal was also found when testing other cluster configurations (e.g., $k = 6, k = 9$). Other studies analysing observational data have reported much larger decreases in translation speed (up to 17% in some regions) (Kossin, 2018), though this finding has been the subject of debate due to various data inhomogeneity issues (Lanzante, 2019; Moon et al., 2019).

3.4. Precipitation and Wind Extremes

Future projections of precipitation and wind extremes associated with TCs and ex-TCs in the southwest Pacific basin are shown in Figure 13. Here we examine intensification across different conditions: TCs in the tropics (blue circles), TCs that have transitioned outside of the tropics (red squares), and TCs that have transitioned outside of the tropics to impact New Zealand (green triangles). Further details of these calculations are provided in Section 2.3. We present each of these as an intensification ratio, defined as the future period TC-related extreme precipitation and wind fields under SSP370 divided by the respective historical period quantities.

For future TC-related precipitation (Figure 13a) under this high emissions scenario the ensemble mean projected increase is approximately 30%–35% across TCs in the tropics and as well as for ex-TCs and those within the New

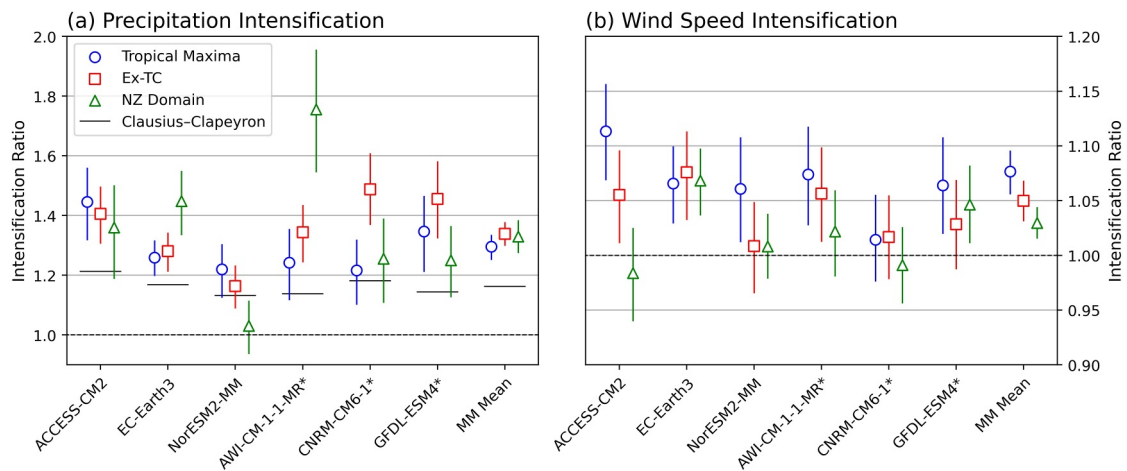


Figure 13. Intensification of precipitation extremes (panel a) and wind speed extremes (panel b) associated with TCs in the future period (years 2070–2099) under SSP370 relative to the historical period (years 1985–2014). Extremes associated with the TC maxima are plotted as blue circles, extremes associated with ex-tropical cyclones are plotted as red squares, and extremes that are associated with ex-tropical cyclones in the NZ domain are plotted as green triangles, with the lines indicating the interquartile range of bootstrap samples. Solid horizontal black lines in panel (a) depict the changes in moisture availability calculated using the Clausius-Clapeyron relation over the tropical domain 25°S–0° on a per-model basis.

Zealand domain. This projected increase is considerably larger than implied by Clausius-Clapeyron scaling, which would be slightly less than 20% for this ensemble/scenario. As shown in Figure 13a, there can be significant differences between models, though most models project larger increases in TC-related precipitation than implied by Clausius-Clapeyron scaling. The rate of warming in each model in this region (as shown in Figure 5 and from the vertical lines in Figure 13) has some bearing on the precipitation intensification, but it is apparent that it is not the sole contributor. For example, CNRM-CM6-1 has a considerably higher warming rate than NorESM2-MM, yet both models have similar precipitation intensification in the tropics (Figure 13). The largest uncertainties (both across models and in the sampling of events within each model) is for ex-TCs within the New Zealand domain, likely stemming from the fact that the intensification ratio is computed from a relatively small number of events (i.e., typically 1–2 events per year, Figure 9).

For future TC-related windspeeds (Figure 13b), the future projected increases are smaller compared to TC-related precipitation. From the ensemble mean, winds are projected to increase by between 3% and 8% depending on the region, with larger increases in the tropics compared to ex-TCs and those impacting New Zealand. For the windspeed intensification rates over New Zealand, some individual models have confidence intervals that span zero (i.e., no change) which likely reflects the smaller sample sizes described above.

Given the relatively high-resolution of CCAM used here (12–30 km), relative to other available model ensembles, our findings provide additional important detail regarding possible future TC and ex-TC impacts in the region. These findings, that relatively large and robust projected changes are evident in TC-related extremes, are consistent with those reported by the IPCC AR6 (Seneviratne et al., 2021) for other TC basins. As is the finding that TC-related precipitation extremes generally show larger and more robust increases than for wind extremes. Although projections of TC frequency were not considered robust for individual Pacific Island nations (discussed earlier in Section 3.2), the magnitude of the precipitation and wind extremes associated with TCs in the tropics presented here provides some general guidance about potential future TC risk for the Islands. Note that we have not presented these projections for individual Island nations due to the smaller sampling of land-falling TCs.

Several existing studies have similarly highlighted the potential for precipitation extremes to scale with warming at rates that exceed Clausius Clapeyron scaling (“super-CC scaling”), though the magnitudes can depend on the region, storm type, sub-daily temporal frequency, and metrics (Ayat et al., 2022; Fowler et al., 2021; Stansfield & Reed, 2023; Wasko et al., 2015). For example, several event attribution studies of major hurricanes impacting the United States have reported super-CC scaling (Patricola & Wehner, 2018; Risser & Wehner, 2017; Van Oldenborgh et al., 2017). Similarly, Reed et al. (2022) reported super-CC scaling of storms in the highly active 2020 North Atlantic hurricane season. For the New Zealand region, Stone et al. (2024) found that peak precipitation intensity could increase by 20%–30% per degree warming for future storms like ex-TC Gabrielle, which is larger

than reported here. In future work, we intend to expand on the aggregated descriptive projections presented here to further investigate mechanisms responsible for differences in the projections reported between regions and models (Figure 13). After accounting for differences in warming rates, the relatively large differences in the projections across the downscaled simulations imply that storm structural dynamics and large-scale circulation (e.g., Stansfield & Reed, 2023; Wasko et al., 2015) are playing an important role from the driving GCM fields.

A caveat to the findings presented here is that although we sample different GCM uncertainty in the projections, the projections are likely also somewhat dependent on the choice and configuration of the dynamical model used for downscaling. Notably, the accurate representation of various model physical processes across scales relevant for TCs remains challenging, including for clouds, convection, boundary-layer processes and air-sea coupling (Roberts et al., 2020a; Sobel et al., 2021; Truong et al., 2025). For example, Truong and Thatcher (2025) detail how the choice of microphysics schemes in CCAM can have important implications on simulated cloud properties and the distribution of precipitation. These factors, alongside model resolution, are highly relevant to the representation of TCs and TC-related precipitation in CCAM (Truong et al., 2025), so continued testing of these sensitivities across higher and variable-resolution grid configurations will be a focus of future work. Furthermore, although the CCAM model resolution used here is in the TC-permitting range (12–30 km), clearly this resolution has limitations given that real world TCs can have eyes less than 10 km, and the ability to capture physically correct high wind intensities is a known model resolution issue (Davis, 2018; Sobel et al., 2021). The configuration of CCAM (i.e., nudged vs. SST-driven) likely also plays a role in determining the properties of simulated TCs; this is difficult to directly quantify from the existing simulations though benefits from bias correcting SSTs are apparent, as discussed earlier. As such, future research performing targeted experiments designed to quantitatively compare these different configurations would be useful. Lastly, since CCAM was run here without coupling to the ocean, any small-scale air-sea interactions relevant for TC projections are not accounted for. As such, these TC projections should be compared and updated as high-performance computing capabilities continue to evolve and newer high-resolution model ensembles become available, such as possible future fully coupled versions of projections from CCAM (e.g., Chapman et al., 2023), HighResMIP2 (Roberts et al., 2024) and other CMIP7 models.

4. Conclusions

Climate projections of TCs are presented here for the southwest Pacific, based on recently produced high-resolution downscaled CMIP6 simulations. The downscaling implements CCAM, a global atmospheric model with a stretched (i.e., variable resolution) grid focusing high resolution over the southwest Pacific and New Zealand. The enhanced resolution spans approximately 12–30-km resolution over the domain, with an average resolution of 22.5-km (Figure 1). Six CMIP6 GCMs are downscaled across the historical period and across the 21st century for SSP126, SSP245, and SSP370 scenarios, equating to approximately 1,800 model simulation years of sub-daily data for TC analysis. Given the combination of ensemble size and resolution, the model ensemble is considered state-of-the-art for examining TC projections across the region.

Previous studies for the region have used regional models driven by prior generations of CMIP3/CMIP5 GCMs (Dutheil et al., 2020; Walsh, 2015). These studies have typically driven regional models by the ensemble mean SST fields of CMIP models, hence cannot explicitly sample and quantify the uncertainty stemming from individual models, which we show here can be large. Other studies have used models within the HighResMIP ensemble (Haarsma et al., 2016) for TC projections globally, hence include the South Pacific region (e.g., Bower & Reed, 2024; Roberts et al., 2020b). A limitation of the HighResMIP ensemble is that only a relatively small number of models are in the “TC permitting” range of resolution (~25-km), and a limited number of years are simulated for this class of models (i.e., the projections extend to year 2050 for a single SSP).

To summarize the main findings of this study, we broadly categorize these into “non-robust projections” and “robust projections” based on model consensus across the downscaled simulations. In terms of non-robust projections, we do not find robust changes in TC frequency across the basin. Projected increases and decreases in TC genesis occur in different sub-regions across models, where the uncertainty in relative SST and tropical convection across the host GCMs appears to be a primary contributor. In terms of ex-tropical TCs, we did not find systematic shifts in the clusters of tracks most relevant to making landfall over New Zealand. Similarly, we did not find robust evidence for poleward shifts in the tracks or overall changes to TC translation speed.

In terms of the more robust projections, the highest intensity TCs (category 4+) are projected to increase in frequency, with 16 of 18 simulations across SSPs and models projecting an increase. This increase in frequency is largest and most consistent under a high-emissions scenario (SSP370). Under SSP370, cluster analysis of TC tracks indicates a slight decrease (in five of six models) in the frequency of storms that preferentially impact northern parts of Australia, or which stay in the tropics (hence do not tend to impact New Zealand). Increases in large-scale subsidence and wind shear across models have likely contributed to this regional decrease in TC frequency. In terms of precipitation extremes associated with TCs, averaged across models these are projected to increase by 30%–35% (depending on the region) under SSP370 by the end-of-century. This increase exceeds Clausius-Clapeyron scaling in five of 6 simulations, both for storms in the tropics and for ex-tropical cyclones impacting New Zealand. Under SSP370, projected extreme windspeeds associated with TCs are smaller compared to precipitation, with increases of between 3% and 8% depending on the region, with larger increases in the tropics compared to ex-TCs and those impacting New Zealand. The smaller sample size for storms which impact New Zealand is likely a contributing factor.

The sensitivity of the results to the driving GCM reported here carries important implications, given that several prior studies have depended on a single GCM or used ensemble (i.e., CMIP) mean projected changes in SSTs to drive regional models. The value of downscaling multiple GCMs has enabled us to explore how projections of these individual environmental conditions differ across GCMs and contribute to uncertainty in TC projections. Narrowing uncertainty in TC projections, especially TC frequency, will therefore require further constraining uncertainty in regional projections of relative SST and tropical convection across the region. Furthermore, it remains extremely challenging to represent TCs in climate model ensembles, given the need to have both sufficiently high atmospheric model resolution and sufficiently long simulations (i.e., number of model years) (Roberts et al., 2020a; Sobel et al., 2021). While the CCAM downscaled ensemble used here provides some improvements in both of these aspects, these TC projections should be compared and updated as high-performance computing capabilities continue to evolve, and newer higher-resolution model ensembles become available.

Conflict of Interest

The authors declare no conflicts of interest relevant to this study.

Data Availability Statement

The ERA5 reanalysis data used in this study are available for download from the Climate Data Store (Hersbach et al., 2023). CMIP6 data used in this study is available from the Earth System Grid Federation (ESGF) archive: <https://esgf-node.llnl.gov/projects/cmip6/>. The CCAM model used here is fully open source and made available by CSIRO: <https://research.csiro.au/ccam/software-and-model-configuration/>. The TempestExtremes package v2.1 used for the detection of TCs is available from Ullrich et al. (2021). The code used to run TempestExtremes, along with example output of tracked TCs, is available and described in an accompanying zenodo repository (Gibson, 2025). The clustering of TC tracks was performed through the open access CCToolbox in MATLAB <http://www.datalab.uci.edu/resources/CCT/doc/>.

Acknowledgments

Funding for this work has been provided by New Zealand's Ministry for Business, Innovation and Employment (MBIE) Building for Climate Change programme contracted through the Ministry for the Environment (MFE contract number 25679). This study was also supported by the MBIE Strategic Science Investment Fund (SSIF). Open access publishing facilitated by National Institute of Water and Atmospheric Research, as part of the Wiley - National Institute of Water and Atmospheric Research agreement via the Council of Australian University Librarians.

References

- Ayat, H., Evans, J. P., Sherwood, S. C., & Soderholm, J. (2022). Intensification of subhourly heavy rainfall. *Science*, 378(6620), 655–659. <https://doi.org/10.1126/science.abn8657>
- Balaguru, K., Leung, L. R., Van Roekel, L. P., Golaz, J.-C., Ullrich, P. A., Caldwell, P. M., et al. (2020). Characterizing tropical cyclones in the energy exascale Earth system model version 1. *Journal of Advances in Modeling Earth Systems*, 12(8), e2019MS002024. <https://doi.org/10.1029/2019MS002024>
- Bhatia, K., Vecchi, G., Murakami, H., Underwood, S., & Kossin, J. (2018). Projected response of tropical cyclone intensity and intensification in a global climate model. *Journal of Climate*, 31(20), 8281–8303. <https://doi.org/10.1175/jcli-d-17-0898.1>
- Bower, E., & Reed, K. A. (2024). Using high resolution climate models to explore future changes in post-tropical cyclone precipitation. *Environmental Research Letters*, 19(2), 024042. <https://doi.org/10.1088/1748-9326/ad2163>
- Brown, J. R., Lengaigne, M., Lintner, B. R., Widlansky, M. J., vander Wiel, K., Dutheil, C., et al. (2020). South Pacific Convergence Zone dynamics, variability and impacts in a changing climate. *Nature Reviews Earth & Environment*, 1(10), 530–543. <https://doi.org/10.1038/s43017-020-0078-2>
- Camargo, S. J., Robertson, A. W., Gaffney, S. J., Smyth, P., & Ghil, M. (2007). Cluster analysis of typhoon tracks. Part I: General properties. *Journal of Climate*, 20(14), 3635–3653. <https://doi.org/10.1175/JCLI4188.1>
- Chand, S. S., Dowdy, A. J., Ramsay, H. A., Walsh, K. J. E., Tory, K. J., Power, S. B., et al. (2019). Review of tropical cyclones in the Australian region: Climatology, variability, predictability, and trends. *WIREs Climate Change*, 10(5), e602. <https://doi.org/10.1002/wcc.602>

- Chapman, S., Syktus, J., Trancoso, R., Thatcher, M., Toombs, N., Wong, K. K. H., & Takbash, A. (2023). Evaluation of dynamically downscaled CMIP6-CCAM models over Australia. *Earth's Future*, 11(1), e2023EF003548. <https://doi.org/10.1029/2023ef003548>
- Chauvin, F., Pilon, R., Palany, P., & Belmadani, A. (2020). Future changes in Atlantic hurricanes with the rotated-stretched ARPEGE-Climat at very high resolution. *Climate Dynamics*, 54(1–2), 947–972. <https://doi.org/10.1007/s00382-019-05040-4>
- Cheung, H. M., & Chu, J.-E. (2023). Global increase in destructive potential of extratropical transition events in response to greenhouse warming. *npj Climate and Atmospheric Science*, 6(1), 137. <https://doi.org/10.1038/s41612-023-00470-8>
- Daloz, A. S., Camargo, S. J., Kossin, J. P., Emanuel, K., Horn, M., Jonas, J. A., et al. (2015). Cluster analysis of downscaled and explicitly simulated north Atlantic tropical cyclone tracks. *Journal of Climate*, 28(4), 1333–1361. <https://doi.org/10.1175/JCLI-D-13-00646.1>
- Davis, C. (2018). Resolving tropical cyclone intensity in models. *Geophysical Research Letters*, 45(4), 2082–2087. <https://doi.org/10.1002/2017gl076966>
- Diamond, H., Lorrey, A., Knapp, K., & Levinson, D. (2011). Development of an enhanced tropical cyclone tracks database for the southwest Pacific from 1840 to 2010. *International Journal of Climatology*, 32(14), 2240–2250. <https://doi.org/10.1002/joc.2412>
- Diamond, H. J., & Renwick, J. (2015a). The climatological relationship between tropical cyclones in the southwest Pacific and the southern annular mode. *International Journal of Climatology*, 35(4), 613–623. <https://doi.org/10.1002/joc.4007>
- Diamond, H. J., Lorrey, A. M., & Renwick, J. A. (2013). A southwest Pacific tropical cyclone climatology and linkages to the El Niño–Southern Oscillation. *Journal of Climate*, 26(1), 3–25. <https://doi.org/10.1175/jcli-d-12-00077.1>
- Diamond, H. J., & Renwick, J. A. (2015b). The climatological relationship between tropical cyclones in the southwest Pacific and the Madden-Julian Oscillation. *International Journal of Climatology*, 35(5), 676–686. <https://doi.org/10.1002/joc.4012>
- Donlon, C. J., Martin, M., Stark, J., Roberts-Jones, J., Fiedler, E., & Wimmer, W. (2012). The operational sea surface temperature and sea ice analysis (OSTIA) system. *Remote Sensing of Environment*, 116, 140–158. <https://doi.org/10.1016/j.rse.2010.10.017>
- Dutheil, C., Lengaigne, M., Bador, M., Vialard, J., Lefèvre, J., Jourdain, N. C., et al. (2020). Impact of projected sea surface temperature biases on tropical cyclones projections in the South Pacific. *Scientific Reports*, 10(1), 4838. <https://doi.org/10.1038/s41598-020-61570-6>
- Erickson, N. E., & Patricola, C. M. (2023). Future projections of the El Niño–Southern Oscillation and tropical Pacific mean State in CMIP6. *Journal of Geophysical Research: Atmospheres*, 128(21), e2022JD037563. <https://doi.org/10.1029/2022JD037563>
- Fowler, H. J., Lenderink, G., Prein, A. F., Westra, S., Allan, R. P., Ban, N., et al. (2021). Anthropogenic intensification of short-duration rainfall extremes. *Nature Reviews Earth & Environment*, 2(2), 107–122. <https://doi.org/10.1038/s43017-020-00128-6>
- Gaffney, S. J., Robertson, A. W., Smyth, P., Camargo, S. J., & Ghil, M. (2007). Probabilistic clustering of extratropical cyclones using regression mixture models. *Climate Dynamics*, 29(4), 423–440. <https://doi.org/10.1007/s00382-007-0235-z>
- Gibson, P. B. (2025). TC tracking code tempest extremes—Southwest Pacific projections. *Zenodo*. [Repository includes code and example of TC tracking]. <https://doi.org/10.5281/zenodo.15620475>
- Gibson, P. B., Rampal, N., Dean, S. M., & Morgenstern, O. (2024). Storylines for future projections of precipitation over New Zealand in CMIP6 models. *Journal of Geophysical Research: Atmospheres*, 129(5), e2023JD039664. <https://doi.org/10.1029/2023jd039664>
- Gibson, P. B., Stone, D., Thatcher, M., Broadbent, A., Dean, S., Rosier, S. M., et al. (2023). High-resolution CCAM simulations over New Zealand and the South Pacific for the detection and attribution of weather extremes. *Journal of Geophysical Research: Atmospheres*, 128(14), e2023JD038530. <https://doi.org/10.1029/2023JD038530>
- Gibson, P. B., Stuart, S., Sood, A., Stone, D., Rampal, N., Lewis, H., et al. (2024). Dynamical downscaling CMIP6 models over New Zealand: Added value of climatology and extremes. *Climate Dynamics*, 62(8), 8255–8281. <https://doi.org/10.1007/s00382-024-07337-5>
- Good, S., Fiedler, E., Mao, C., Martin, M. J., Maycock, A., Reid, R., et al. (2020). The current configuration of the OSTIA system for operational production of foundation sea surface temperature and ice concentration analyses. *Remote Sensing*, 12(4), 720. <https://doi.org/10.3390/rs12040720>
- Haarsma, R. J., Roberts, M. J., Vidale, P. L., Senior, C. A., Bellucci, A., Bao, Q., et al. (2016). High resolution model intercomparison project (HighResMIP v1. 0) for CMIP6. *Geoscientific Model Development*, 9(11), 4185–4208. <https://doi.org/10.5194/gmd-9-4185-2016>
- Harrington, L. J., Dean, S. M., Awatere, S., Rosier, S., Queen, L., Gibson, P. B., et al. (2023). The role of climate change in extreme rainfall associated with cyclone Gabrielle over Aotearoa new Zealand's east coast.
- Hersbach, H., Bell, B., Barrisford, P., Hirahara, S., Biavati, G., & Horányi, A. (2023). ERA5 hourly data on pressure levels from 1940 to present [Dataset]. *Copernicus Climate Change Service (C3S) Climate Data Store (CDS)*. <https://doi.org/10.24381/cds.bd0915c6>
- Hersbach, H., Bell, B., Berrisford, P., Hirahara, S., Horányi, A., Muñoz-Sabater, J., et al. (2020). The ERA5 global reanalysis. *Quarterly Journal of the Royal Meteorological Society*, 146(730), 1999–2049. <https://doi.org/10.1002/qj.3803>
- Hodges, K., Cobb, A., & Vidale, P. L. (2017). How well are tropical cyclones represented in reanalysis datasets? *Journal of Climate*, 30(14), 5243–5264. <https://doi.org/10.1175/jcli-d-16-0557.1>
- Hoffmann, P., Katzfey, J., McGregor, J., & Thatcher, M. (2016). Bias and variance correction of sea surface temperatures used for dynamical downscaling. *Journal of Geophysical Research: Atmospheres*, 121(21), 12877–12890. <https://doi.org/10.1002/2016jd025383>
- Hoyos, C. D., & Webster, P. J. (2012). Evolution and modulation of tropical heating from the last glacial maximum through the twenty-first century. *Climate Dynamics*, 38(7–8), 1501–1519. <https://doi.org/10.1007/s00382-011-1181-3>
- Johnson, N. C., & Xie, S.-P. (2010). Changes in the sea surface temperature threshold for tropical convection. *Nature Geoscience*, 3(12), 842–845. <https://doi.org/10.1038/ngeo1008>
- Klotzbach, P. J., Bell, M. M., Bowen, S. G., Gibney, E. J., Knapp, K. R., & Schreck, C. J. (2020). Surface pressure a more skillful predictor of normalized hurricane damage than maximum sustained wind. *Bulletin of the American Meteorological Society*, 101(6), E830–E846. <https://doi.org/10.1175/BAMS-D-19-0062.1>
- Knapp, K. R., Diamond, H. J., Kossin, J. P., Kruk, M. C., & Schreck, C. J. (2018). *International best track archive for climate stewardship (IBTrACS) project, version 4* (Vol. 10). NOAA National Centers for Environmental Information.
- Knutson, T. R., Camargo, S. J., Chan, J. C., Emanuel, K., Ho, C.-H., Kossin, J., et al. (2020). Tropical cyclones and climate change assessment: Part II: Projected response to anthropogenic warming. *Bulletin of the American Meteorological Society*, 101(3), E303–E322. <https://doi.org/10.1175/bams-d-18-0194.1>
- Knutson, T. R., Sirutis, J. J., Bender, M. A., Tuleya, R. E., & Schenkel, B. A. (2022). Dynamical downscaling projections of late twenty-first-century US landfalling hurricane activity. *Climatic Change*, 171(3), 28. <https://doi.org/10.1007/s10584-022-03346-7>
- Kossin, J. P. (2018). A global slowdown of tropical-cyclone translation speed. *Nature*, 558(7708), 104–107. <https://doi.org/10.1038/s41586-018-0158-3>
- Lanzante, J. R. (2019). Uncertainties in tropical-cyclone translation speed. *Nature*, 570(7759), E6–E15. <https://doi.org/10.1038/s41586-019-1223-2>
- Lorrey, A. M., Griffiths, G., Fauchereau, N., Diamond, H. J., Chappell, P. R., & Renwick, J. (2014). An ex-tropical cyclone climatology for Auckland, New Zealand. *International Journal of Climatology*, 34(4), 1157–1168. <https://doi.org/10.1002/joc.3753>

- Ma, W., Chen, G., & Guan, B. (2020). Poleward shift of atmospheric Rivers in the Southern hemisphere in recent decades. *Geophysical Research Letters*, 47(21), e2020GL089934. <https://doi.org/10.1029/2020GL089934>
- Mendelsohn, R., Emanuel, K., Chonabayashi, S., & Bakkenes, L. (2012). The impact of climate change on global tropical cyclone damage. *Nature Climate Change*, 2(3), 205–209. <https://doi.org/10.1038/nclimate1357>
- Moon, I.-J., Kim, S.-H., & Chan, J. C. L. (2019). Climate change and tropical cyclone trend. *Nature*, 570(7759), E3–E5. <https://doi.org/10.1038/s41586-019-1222-3>
- Muller, J., Mooney, K., Bowen, S. G., Klotzbach, P. J., Martin, T., Philp, T. J., et al. (2025). Normalized Hurricane damage in the United States: 1900–2022. *Bulletin of the American Meteorological Society*, 106(1), E51–E67. <https://doi.org/10.1175/BAMS-D-23-0280.1>
- Murakami, H., Cooke, W. F., Mizuta, R., Endo, H., Yoshida, K., Wang, S., & Hsu, P.-C. (2024). Robust future projections of global spatial distribution of major tropical cyclones and sea level pressure gradients. *Communications Earth & Environment*, 5(1), 479. <https://doi.org/10.1038/s43247-024-01644-9>
- Nakamura, J., Camargo, S. J., Sobel, A. H., Henderson, N., Emanuel, K. A., Kumar, A., et al. (2017). Western North Pacific tropical cyclone model tracks in present and future climates. *Journal of Geophysical Research: Atmospheres*, 122(18), 9721–9744. <https://doi.org/10.1002/2017JD027007>
- Patricola, C. M., & Wehner, M. F. (2018). Anthropogenic influences on major tropical cyclone events. *Nature*, 563(7731), 339–346. <https://doi.org/10.1038/s41586-018-0673-2>
- Reed, K., Wehner, M., & Zarzycki, C. (2022). Attribution of 2020 hurricane season extreme rainfall to human-induced climate change. *Nature Communications*, 13(1), 1905. <https://doi.org/10.1038/s41467-022-29379-1>
- Risser, M. D., & Wehner, M. F. (2017). Attributable human-induced changes in the likelihood and magnitude of the observed extreme precipitation during Hurricane Harvey. *Geophysical Research Letters*, 44(24), 12457–12464. <https://doi.org/10.1002/2017gl075888>
- Roberts, M. J., Camp, J., Seddon, J., Vidale, P. L., Hodges, K., Vannière, B., et al. (2020a). Impact of model resolution on tropical cyclone simulation using the HighResMIP–PRIMAVERA multimodel ensemble. *Journal of Climate*, 33(7), 2557–2583. <https://doi.org/10.1175/jcli-d-19-0639.1>
- Roberts, M. J., Camp, J., Seddon, J., Vidale, P. L., Hodges, K., Vannière, B., et al. (2020b). Projected future changes in tropical cyclones using the CMIP6 HighResMIP multimodel ensemble. *Geophysical Research Letters*, 47(14), e2020GL088662. <https://doi.org/10.1029/2020GL088662>
- Roberts, M. J., Reed, K. A., Bao, Q., Barsugli, J. J., Camargo, S. J., Caron, L. P., et al. (2024). High resolution model intercomparison project phase 2 (HighResMIP2) towards CMIP7. *EGUsphere*, 2024, 1–41. <https://doi.org/10.5194/egusphere-2024-2582>
- Schroeter, B. J., Ng, B., Takbash, A., Rafter, T., & Thatcher, M. (2024). A comprehensive evaluation of mean and extreme climate for the conformal cubic atmospheric model (CCAM). *Journal of Applied Meteorology and Climatology*, 63(9), 997–1018. <https://doi.org/10.1175/jamc-d-24-0004.1>
- Seneviratne, S. I., Zhang, X., Adnan, M., Badi, W., Dereczynski, C., Di Luca, A., et al. (2021). Weather and climate extreme events in a changing climate. In *Climate Change 2021: The Physical Science Basis. Contribution of Working Group I to the Sixth Assessment Report of the Intergovernmental Panel on Climate Change*. <https://doi.org/10.1017/9781009157896.013>
- Sinclair, M. R. (2002). Extratropical transition of Southwest Pacific tropical cyclones. Part I: Climatology and mean structure changes. *Monthly Weather Review*, 130(3), 590–609. [https://doi.org/10.1175/1520-0493\(2002\)130<0590:ETOSPT>2.0.CO;2](https://doi.org/10.1175/1520-0493(2002)130<0590:ETOSPT>2.0.CO;2)
- Sobel, A. H., Lee, C.-Y., Bowen, S. G., Camargo, S. J., Cane, M. A., Clement, A., et al. (2023). Near-term tropical cyclone risk and coupled Earth system model biases. *Proceedings of the National Academy of Sciences of the United States of America*, 120(33), e2209631120. <https://doi.org/10.1073/pnas.2209631120>
- Sobel, A. H., Wing, A. A., Camargo, S. J., Patricola, C. M., Vecchi, G. A., Lee, C. Y., & Tippett, M. K. (2021). Tropical cyclone frequency. *Earth's Future*, 9(12), e2021EF002275. <https://doi.org/10.1029/2021ef002275>
- Stansfield, A. M., & Reed, K. A. (2023). Global tropical cyclone precipitation scaling with sea surface temperature. *npj Climate and Atmospheric Science*, 6(1), 60. <https://doi.org/10.1038/s41612-023-00391-6>
- Stone, D. A., Noble, C. J., Bodeker, G. E., Dean, S. M., Harrington, L. J., Rosier, S. M., et al. (2024). Cyclone Gabrielle as a design storm for northeastern Aotearoa New Zealand under anthropogenic warming. *Earth's Future*, 12(9), e2024EF004772. <https://doi.org/10.1029/2024ef004772>
- Teng, H., & Branstator, G. (2017). Causes of extreme ridges that induce California droughts. *Journal of Climate*, 30(4), 1477–1492. <https://doi.org/10.1175/jcli-d-16-0524.1>
- Thatcher, M., & McGregor, J. L. (2009). Using a scale-selective filter for dynamical downscaling with the conformal cubic atmospheric model. *Monthly Weather Review*, 137(6), 1742–1752. <https://doi.org/10.1175/2008mwr2599.1>
- Truong, S. C. H., Ramsay, H. A., Rafter, T., & Thatcher, M. J. (2025). Simulation of an intense tropical cyclone in the conformal cubic atmospheric model and its sensitivity to horizontal resolution. *Weather and Climate Extremes*, 47, 100744. <https://doi.org/10.1016/j.wace.2025.100744>
- Truong, S. C. H., & Thatcher, M. (2025). Evaluation of clouds in the conformal cubic atmospheric model using the CFMIP observation simulator package. *International Journal of Climatology*, 45(8), e8846. <https://doi.org/10.1002/joc.8846>
- Ullrich, P. A., Zarzycki, C. M., McClenny, E. E., Pinheiro, M. C., Stansfield, A. M., & Reed, K. A. (2021). TempestExtremes v2. 1: A community framework for feature detection, tracking, and analysis in large datasets. *Geoscientific Model Development*, 14(8), 5023–5048. <https://doi.org/10.5194/gmd-14-5023-2021>
- Van Oldenborgh, G. J., Van Der Wiel, K., Sebastian, A., Singh, R., Arrighi, J., Otto, F., et al. (2017). Attribution of extreme rainfall from Hurricane Harvey, August 2017. *Environmental Research Letters*, 12(12), 124009. <https://doi.org/10.1088/1748-9326/aa9ef2>
- Walsh, K. J. E. (2015). Fine resolution simulations of the effect of climate change on tropical cyclones in the South Pacific. *Climate Dynamics*, 45(9–10), 2619–2631. <https://doi.org/10.1007/s00382-015-2497-1>
- Walsh, K. J. E., McInnes, K. L., & McBride, J. L. (2012). Climate change impacts on tropical cyclones and extreme sea levels in the South Pacific – A regional assessment. *Global and Planetary Change*, 80, 149–164. <https://doi.org/10.1016/j.gloplacha.2011.10.006>
- Wasko, C., Sharma, A., & Johnson, F. (2015). Does storm duration modulate the extreme precipitation-temperature scaling relationship? *Geophysical Research Letters*, 42(20), 8783–8790. <https://doi.org/10.1002/2015GL066274>
- Wehner, M. F., Reed, K. A., Li, F., Prabhat, Bacmeister, J., Chen, C.-T., et al. (2014). The effect of horizontal resolution on simulation quality in the Community Atmospheric Model, CAM5.1. *Journal of Advances in Modeling Earth Systems*, 6(4), 980–997. <https://doi.org/10.1002/2013MS000276>
- Wilson, N., Broadbent, A., & Kerr, J. (2023). *Cyclone Gabrielle by the numbers—A review at six months*. Public Health Communication Centre. Retrieved from <https://www.phcc.org.nz/briefing/cyclone-gabrielle-numbers-review-six-months>

- Zhang, W., Villarini, G., Scoccimarro, E., Roberts, M., Vidale, P. L., Vanniere, B., et al. (2021). Tropical cyclone precipitation in the HighResMIP atmosphere-only experiments of the PRIMAVERA Project. *Climate Dynamics*, 57(1–2), 253–273. <https://doi.org/10.1007/s00382-021-05707-x>
- Zhuo, J.-Y., Lee, C.-Y., Sobel, A., Seager, R., Camargo, S. J., Lin, Y.-H., et al. (2025). A More La Niña–Like Response to Radiative Forcing after Flux Adjustment in CESM2. *Journal of Climate*, 38(4), 1037–1050. <https://doi.org/10.1175/JCLI-D-24-0331.1>